

1 Interannual variability of the initiation of the phytoplankton 2 growing period in two French coastal ecosystems

3 Coline Poppeschi¹, Guillaume Charria¹, Anne Daniel², Romaric Verney³, Peggy Rimmelin-
4 Maury⁴, Michaël Retho⁵, Eric Goberville⁶, Emilie Grossteffan⁴, Martin Plus²

5 ¹Ifremer, Univ. Brest, CNRS, IRD, Laboratory for Ocean Physics and Satellite remote sensing (LOPS), IUEM,
6 29280 Brest, France.

7 ²Ifremer, DYNECO, Pelagic Ecology Laboratory (PELAGOS), 29280 Brest, France.

8 ³Ifremer, DYNECO, Hydrosedimentary Dynamics Laboratory (DHYSED), 29280 Brest, France.

9 ⁴OSU-European University Institute of the Sea (IUEM), UMS3113, 29280 Plouzané, France.

10 ⁵Ifremer, Morbihan-Pays de Loire Environment Resources Laboratory (LERMPL), 56100 Lorient, France.

11 ⁶Unité Biologie des Organismes et Écosystèmes Aquatiques (BOREA), Muséum National d'Histoire Naturelle,
12 CNRS, IRD, Sorbonne Université, Université de Caen Normandie, Université des Antilles, Paris, France

13 *Correspondence to:* Coline Poppeschi (coline.poppeschi@ifremer.fr)

14 *Main manuscript modifications are highlighted in red.*

15 **Abstract.** Decadal time series of chlorophyll-*a* concentrations sampled at high and low frequencies are explored
16 to study **climate-induced impacts on** the processes inducing interannual variations in the Initiation of the
17 Phytoplankton Growing Period (IPGP) in early spring. We specifically detail the IPGP in two contrasting coastal
18 temperate ecosystems under the influence of rivers highly rich in nutrients: the Bay of Brest and the Bay of Vilaine.
19 **In both coastal ecosystems, we observed a large interannual variation in IPGP influenced by sea temperature, river**
20 **inputs, light availability (modulated by solar radiation and water turbidity), and turbulent mixing generated by**
21 **tidal currents, wind stress and river runoff.** We show that the IPGP is delayed by around 30 days in 2019 in
22 comparison with 2010. *In situ* observations and a one-dimensional vertical model coupling hydrodynamics,
23 biogeochemistry, and sediment dynamics, show that the IPGP generally not depends on one specific environmental
24 factor, but on the interaction between several environmental factors. In these two bays, we demonstrate that IPGP
25 is mainly caused by sea surface temperature and available light conditions, mostly controlled by the turbidity of
26 the system before first blooms. While both bays are hydrodynamically contrasted, the processes that modulate
27 IPGP are similar. In both bays, IPGP can be delayed by cold spells and flood events at the end of winter, provided
28 that these extreme events last several days.

30 **Keywords**

31 Phytoplankton biomass, Long-term *in situ* observations, Coastal temperate ecosystems, Extreme events, Climate
32 change.

33 **1 Introduction**

34 Although studied for 70 years (Sverdrup, 1953), the optimal conditions that trigger the Initiation of
35 Phytoplankton Growing Period (IPGP) in ocean waters in early spring are not well understood (Sathyendranath *et*
36 *al.*, 2015). Three main theories are proposed to date: the Critical Depth Hypothesis (Sverdrup, 1953), the Critical
37 Turbulence Hypothesis (Huisman *et al.*, 1999) and the Disturbance-Recovery Hypothesis (Banse, 1994;
38 Behrenfeld, 2010; Behrenfeld *et al.*, 2013). **For Sverdrup (1953), phytoplankton blooms occur when surface mixed**
39 **layer shoals to a depth shallower than the critical depth, according to light conditions. While Huisman *et al.* (1999)**
40 **agreed with Sverdrup, he proposed that relaxation of turbulent mixing allows bloom to develop if it occurs below**
41 **a critical turbulence rate. Behrenfeld (2010) observed blooms in the absence of spring mixed layer shoaling, and**
42 **declared that the initiation of bloom is controlled by a balance between phytoplankton growth and grazing rate,**
43 **and suggested a seasonal control of this balance by physical processes. No consensus emerges among these**
44 **hypotheses – especially because most of these concepts have been defined at specific temporal and spatial scales**
45 **(Caracciolo *et al.*, 2021; Chiswell *et al.*, 2015) – and the debate is still open, in particular due to the use of more**
46 **efficient models, the availability of new observations, and the ensuing collection of large *in situ* datasets (Boss and**
47 **Behrenfeld, 2010; Rumyantseva *et al.*, 2019). Coastal waters remain highly dynamic and productive ecosystems**

48 at the interface between land and sea, and are distinguished from the waters of the open sea (Gohin *et al.*, 2019;
49 Liu *et al.*, 2019). Because coastal systems are directly influenced by anthropogenic inputs from rivers, no nutrient
50 limitation is observed in late winter. A myriad of factors and mechanisms can then affect the IPGP in coastal areas
51 (Townsend *et al.*, 1994; Cloern, 1996), but the incident light at the air/sea interface (Glé *et al.*, 2007) and Sea
52 Surface Temperature (SST) (Trombetta *et al.*, 2019) are considered as the main forcings. Low water turbidity also
53 plays an important role, and allows deeper light penetration (Iriarte and Purdie, 2004). This occurs by low vertical
54 mixing conditions in shallow waters (Ianson *et al.*, 2001), *i.e.* limited advective exchanges, weak wind (Tian *et al.*,
55 2011), neap tide (Ragueneau *et al.*, 1996), and in absence of flooding events (Peierls *et al.*, 2012). Depending
56 on the morphology and hydrodynamics of coastal zones (estuaries, bays, lagoons), the importance of controlling
57 factors can be variable (Cloern, 1996). **Temporal variation in IPGP** is of great importance in coastal ecosystems
58 because it impacts not only phytoplankton by changing species composition or the succession of species (Ianson
59 *et al.*, 2001; Edwards and Richardson, 2004; Chivers *et al.*, 2020), but also several other biological compartments,
60 such as zooplankton and fish, by species replacements (Sommer *et al.*, 2012).

61
62 By amplifying or modifying environmental forcings, it is now well-documented that global climate
63 change may influence the IPGP in coastal areas (Smetacek and Cloern, 2008; Barbosa *et al.*, 2010; Pearl *et al.*,
64 2014; IPCC, 2021). Heat waves - as opposed to cold spells - have become more frequent in recent years and can
65 advance or delay the IPGP (Gomez and Souissi, 2008). Wind storms, by inducing vertical mixing and sediment
66 resuspension, can have a significant effect on water turbidity, which in turn limits light penetration and therefore
67 influences the IPGP. Floods, following heavier rainfall, may increase continental erosion and ultimately nutrient
68 inputs to coastal ecosystems. Because coastal ecosystems are strongly influenced by human activities such as
69 changes in land use, quantifying the contribution related to long-term climate-induced signals is challenging
70 (Krompkamp and Van Engeland, 2010).

71
72 Our study is based on two geographically close, but hydrodynamically different, nearshore ecosystems:
73 (1) the Bay of Brest, a shallow semi-enclosed bay with well-mixed waters (Le Pape and Menesguen, 1997) and
74 (2) the Bay of Vilaine, a shallow open bay with long water residence times (Chapelle *et al.*, 1994). These two
75 coastal ecosystems are strongly impacted by anthropogenic pressures, such as intensive agriculture (Ragueneau *et al.*,
76 2018; Ratmaya *et al.*, 2019), which induces highly rich nutrient waters.

77
78 In this study, we aim to better understand interannual local changes in the IPGP in coastal temperate
79 ecosystems in the current context of global climate change over the last 20 years. As most studies dealing with
80 IPGP are mainly based on discrete water sampling (Iriarte *et al.*, 2004; Tian *et al.*, 2011) or modeling (Townsend
81 *et al.*, 1994; Philippart *et al.*, 2010), we focus here on the use of long-term high-frequency observations to assess
82 interannual variability of the IPGP, and to identify the triggering and controlling factors. We detect and analyze
83 the temporal variability of the IPGP and quantify how environmental forcings influence its dynamics. To detect
84 and analyze IPGP in coastal environments, we develop a numerical framework that combines high-frequency
85 decadal *in situ* observations and a one-dimensional vertical (1DV) hydro-sedimentary and biogeochemical coupled
86 numerical model. The potential impact of hydro-meteorological extreme events, such as cold spells, flood events
87 and wind bursts, on the IPGP is then investigated.

88 89 90 **2 Data and methods**

91 92 **2.1 Study areas**

93
94 **Our study focuses on two northwestern French coastal temperate ecosystems located in the Bay of Biscay,**
95 **the Bay of Brest and the Bay of Vilaine, two ecosystems impacted by excessive nutrient inputs from watersheds,**
96 **but exposed to different hydrodynamic conditions.**

97
98 **The Bay of Biscay is a region with a complex system of coastal currents influenced by the combined**
99 **effects of seasonal wind regimes and important river discharges modulated by large-scale gyre circulation patterns**
100 **(Ferrer *et al.*, 2009; Lazure and Jégou, 1998; Lazure *et al.*, 2006; Isemer and Hasse, 1985; Pingree and Le Cann,**
101 **1989, 1990; Le Boyer *et al.*, 2013; Lazure *et al.*, 2006; Charria *et al.*, 2013). In the Iroise Sea, at spring tide close**
102 **to the islands and capes, tidal currents can reach 4 m s^{-1} (Muller *et al.*, 2010). This tidal circulation combined with**
103 **meteorological forcings and sharp thermal gradients generate a strongly variable local circulation. In the vicinity**
104 **of the Loire estuary, the freshwater discharges in the surface layers induce important density gradients driving a**
105 **poleward circulation (about 10 cm s^{-1}) modulated by wind forcings (Lazure and Jégou, 1998; Lazure *et al.*, 2006).**
106 **The river plumes can propagate under specific conditions towards the South-West.**

108
109 Under these hydrodynamic conditions, the Bay of Brest is a semi-enclosed bay (180 km²) with 50% of
110 the surface shallower than 5 m depth. The Bay is connected with the Atlantic Ocean (Iroise sea) through a narrow
111 and shallow strait. Tidal variation reaches 8 m during spring tides, which represents an oscillating volume of 40%
112 of the high tide volume. Freshwater inputs come from the Aulne river (catchment area 1875 km², mean river flow
113 26 m³ s⁻¹), and two smaller rivers, the Elorn (catchment area 385 km², mean river flow 6 m³ s⁻¹) and the Mignonne
114 (catchment area 111 km², mean river flow 1.5 m³ s⁻¹). **Due to the macrotidal regime, associated with a strong
115 vertical mixing, the high nitrate concentrations do not generate important green tides (Le Pape *et al.*, 1997). Strong
116 decreases in the Si:N and Si:P ratios did not exhibit dramatic phytoplankton community shifts from diatoms to
117 non-siliceous species in spring (Del Amo *et al.*, 1997), because of the high Si recycling (Ragueneau *et al.*, 2002;
118 Beucher *et al.*, 2004).**

119
120 The Bay of Vilaine is a mesotidal open bay (69 km²) under the influence of the Vilaine (catchment area
121 10 500 km², mean river flow 70 m³ s⁻¹) and the Loire (catchment area 117 000 km², mean river flow 850 m³ s⁻¹)
122 river discharges, with tidal ranges varying between 4 and 6 m (Merceron, 1985). The Loire river plume tends to
123 spread northwestward, with a dilution of 20- to 100-fold by the time it reaches the Bay of Vilaine (Ménésguen
124 *et al.*, 2018). The Vilaine river plume tends to spread throughout the bay before moving westward (Chapelle *et al.*,
125 1994). The water residence time varies seasonally between 10 and 20 days (Chapelle *et al.*, 1994). The water
126 circulation is mainly driven by tides, winds and river flows (Lazure and Jegou, 1998). This bay is well known as
127 one of the most sensitive European Atlantic coastal ecosystems to eutrophication (Ménésguen *et al.*, 2019). The
128 Bay of Vilaine has undergone eutrophication over recent decades mainly due to high nutrient inputs from the
129 Vilaine and Loire rivers (Rossignol-Strick, 1985; Ratmaya *et al.*, 2019).

130 2.2 *In situ* observations

131
132 COAST-HF-Iroise (Rimmelin-Maury *et al.*, 2020) and COAST-HF-Molit (Retho *et al.*, 2020) are two high-
133 frequency monitoring buoys of the French national observation network COAST-HF¹ (Répécaud *et al.*, 2019;
134 Farcy *et al.*, 2019; Cocquempot *et al.*, 2019; Poppeschi *et al.*, 2021) located respectively in the Bay of Brest
135 (4.582°W; 48.357°N) and in the Bay of Vilaine (2.660°W; 47.434°N) (Fig. 1). COAST-HF-Iroise has been
136 operating in the strait between the Bay of Brest and the Iroise sea since 2000. COAST-HF-Molit buoy has been
137 sampling the plume of the Vilaine river since 2008. Buoys are deployed during the whole year except for COAST-
138 HF-Molit that is only available for part of the year prior to 2018 (from mid-February to early September, i.e. from
139 day 50 to 250 for the period 2008-2017). Depending on the tide, the depth at the mooring sites ranges from 11 to
140 17 m for both COAST-HF buoys. **Environmental parameters (SST, salinity, turbidity, dissolved oxygen and Chl-
141 a fluorescence) are measured at 1 to 2 m below the surface every 20 minutes (COAST-HF-Iroise) or every hour
142 (COAST-HF-Molit).** The Chl-*a* fluorescence, a proxy of phytoplankton biomass (FFU unit), is measured by a
143 Turner CYCLOPS-7 Sensor (precision \pm 5%).

144 Sub-surface Chl-*a* concentrations are provided by two French marine monitoring networks, the SOMLIT
145 coastal observation network² and the REPHY (French Observation and Monitoring program for Phytoplankton
146 and Hydrology in coastal waters)³. Samples are collected bimonthly at the SOMLIT-Brest (4.552°W; 48.358°N)
147 and the REPHY-Loscolo (2.445°W; 47.496°N) stations, which are close to the COAST-HF stations. Chl-*a*
148 concentrations are measured with either spectrophotometric or fluorimetric methods (Aminot and Kérouel, 2004).
149

150 Daily river flows are measured at gauging stations (French hydrology “Banque Hydro” database⁴), located
151 close to the main river mouths [Aulne-Gouezec (4.093°W; 48.205°N), Loire-Montjean (1.78°W; 47.106°N)]. The
152 Vilaine river flow is controlled by a dam, and data are provided by the Vilaine Public Territorial Basin
153 Organization⁵ (Fig. 1).
154

¹ www.coast-hf.fr, data available on www.coriolis-cotier.org

² <https://somlit.fr>

³ <https://doi.org/10.17882/47428>

⁴ www.hydro.eaufrance.fr/

⁵ <https://www.eptb-vilaine.fr/>

⁶ <https://donneespubliques.meteofrance.fr/>

⁷ <http://data.shom.fr>

155 The tide gauge stations (Shom⁷) at Brest (4.495°W; 48.382°N) and Crouesty (2.895°W; 47.542°N) record the
156 sea level every minute.

157
158 Precipitation, air temperature, wind direction and intensity, and the solar flux data are retrieved every 6 minutes
159 from two meteorological stations from the Météo-France observation network⁶: Guipavas (4.410°W; 48.440°N)
160 and Vannes-Séné (2.425°W; 47.362°N) (Fig. 1). We use the solar flux as a proxy for subsurface PAR
161 (Photosynthetically Available Radiation).

162 2.3 MARS3D-1DV modeling experiments

163 2.3.1 MARS3D-1DV model

164
165 A 1DV (one-dimensional vertical) model configuration is implemented to simulate changes in biogeochemical
166 variables due to hydrodynamics and sediment dynamics in both bays.

167
168 The hydrodynamical model is based on the code developed for MARS3D (3D hydrodynamics Model for
169 Applications at Regional Scale; Lazure and Dumas, 2008). This model is a primitive equation model with a free
170 surface and uses the Boussinesq and hydrostatic pressure assumptions. We use the 1DV configuration of the
171 model, with 10 vertical sigma levels for 15 m depth and a time step of 30s.

172
173 The sediment model (MUSTANG - Le Hir *et al.*, 2011; Grasso *et al.*, 2015; Mengual *et al.*, 2017) is designed
174 to simulate the transport and changes in different sediment mixtures. In the sediment, 50 layers (refined near the
175 surface) for a total thickness of 40 cm are implemented. Four sediment classes are considered: muds (diameter 10
176 μm), fine sand (diameter 100 μm), medium sand (diameter 200 μm) and coarse sand (diameter 400 μm). The
177 sediment dynamics (transport in the water column, exchanges at the water/sediment interface, erosion/deposition
178 processes) are driven by an advection/dispersion equation for each sediment class (refer to Le Hir *et al.*, 2011 for
179 a detailed description of the sediment model).

180
181 The biogeochemical model BLOOM (Biogeochemical cOastal Ocean Model) is derived from the ECO-
182 MARS model (Cugier *et al.*, 2005; Ménesguen *et al.*, 2019) adding major processes of early diagenesis. Nitrogen,
183 phosphorus, and silica cycles are studied considering four nutrients: nitrate, ammonium, soluble reactive
184 phosphorus and silicic acid (sorption/desorption of phosphate on suspended sediment and precipitation/dissolution
185 of phosphate with iron processes are also included). The model is also represented by three phytoplankton classes
186 (microphytoplankton, dinoflagellates, pico-nano-phytoplankton), two zooplankton classes (micro- and meso-
187 zooplankton), and exchanges at the water/sediment interface and inside the sediment compartment.

188 2.3.2 MARS3D-1DV model sensitivity experiments

189
190 These three models (hydrodynamical, sediment and biogeochemical) are coupled online during simulations
191 and allow the nutrient and phytoplankton dynamics in both bays to be reproduced. The simulation for the Bay of
192 Brest does not include nutrient inputs from the sediment because it is considered to be negligible around the
193 COAST-HF-Iroise station.

194
195 Dissolved and particulate variables are defined in the water column and in the sediment. Initial values for both
196 bays are uniform over the initial vertical profile (Table 1) and are based on a 3D realistic coupled simulation during
197 the year 2015. Values for the 15th of February are extracted at the position of COAST-HF-Iroise for the Bay of
198 Brest and at the position of COAST-HF-Molit station for the Bay of Vilaine (Plus *et al.*, 2021).

199
200 To evaluate the sensitivity of the biogeochemical dynamics to environmental conditions, sensitivity
201 experiments are then performed using the coupled MARS3D/BLOOM/MUSTANG 1DV model configuration. All
202 simulations are started at the end of winter (15th February) and run until the end of the year. The range of values
203 used in the sensitivity experiments are derived from the minimum and maximum observed *in situ* data. Each
204 parameter is tested with a constant value for the whole simulation.

205
206 Three parameters are individually explored in both bays:

- 207 - The air temperature in sensitivity experiments ranges from 4 to 14°C and is controlled by the intensity of
208 solar radiations. Air temperature represents the main controlling parameter of SST in the 1DV model. This
209 parameter drives the radiative fluxes in the model and then constrains SST.

- 210 - Wind intensity effect on the IPGP is explored for values between 0 and 10 m s⁻¹. In the 1DV model, wind
211 is a source of vertical mixing in the simulation.
212 - The Cloud Coverage (CC) sensitivity experiments ranged in value between 0 and 100% CC. This
213 parameter is a driver of Photosynthetic Available Radiation (PAR) in the ocean. For the formulation of
214 radiative fluxes in the 1DV MARS3D model, 100% cloud coverage allows an inflow of 38% of the total
215 solar radiation in the water column. Each individual experiment is associated with a constant CC applied
216 to the seasonal solar radiation.
217

218 In the Bay of Vilaine, the sediment plays a role on light penetration and acts as an active source of nutrients: we
219 therefore explored the influence of mud erosion rate (values between 2.10⁻⁵ and 2.10⁻⁷ kg m⁻² s⁻¹) in that bay (sand
220 erosion rate fixed to 0.0001 kg m⁻² s⁻¹). For the sensitivity experiments, it drives a mass of sediment eroded and
221 resuspended and a bottom input of nutrients in the water column.
222

223 A second set of experiments is conducted by combining the individual effect of environmental parameters in order
224 to explore possible cumulative or opposite effects on the IPGP. The upper and lower bounds of the range of
225 environmental parameters are taken into account. Experiments are detailed in Table 5.

226 2.4 Data processing

227 2.4.1 Chl-*a* fluorescence data

228 To analyze high-frequency time series of *in situ* Chl-*a* fluorescence, the Quenching effect (Lehmuskero
229 *et al.*, 2018) - a decrease in fluorescence in the presence of light (Fig. 2) - is removed by analyzing only night-time
230 data, as reported in Carberry *et al.* (2019). Chl-*a* fluorescence data are studied on a daily basis, i.e. averaged from
231 10 pm to 5 am. Years with less than 75% of valid data are not considered in our analyses: for the Bay of Brest,
232 2005, 2006, 2008, 2009 and 2018.
233

234 2.4.2 Detection of the IPGP

235 On the basis of literature, we first apply three methods to determine the annual IPGP dates:
236 - (1) Set an arbitrary beginning and end of the phytoplankton growing period at 20% and 80% of the
237 cumulative Chl-*a* fluorescence measured from January 1st to December 31st (Kromkamp *et al.*, 2010).
238 - (2) Consider a threshold of 5% above the yearly median chlorophyll (Brody *et al.*, 2013).
239 - (3) Consider the beginning of the growing period as the maximum daily difference in Chl-*a* fluorescence
240 (Philippart *et al.*, 2010).
241
242

243 Because none of these methods allowed us to obtain a valid IPGP detection - **with a too late (method 1)**
244 **or a too early (method 2) detection**, or multiple IPGP dates (method 3) - we elaborate a detection method based on
245 discontinuities of the Chl-*a* fluorescence signal (Fig. 3): daily FFU slopes are calculated based on a linear
246 regression over a ± 2 day window for each day, from 1st January to 31st December, and each year. The IPGP date
247 is identified when the slope exceeds a threshold value - defined as the median of the daily slopes - for the first time
248 in the year for at least 20 days. The end of the phytoplankton growing period is determined when the slope
249 stabilizes below the threshold for at least 20 days for the last time in the year. The cumulative Chl-*a* fluorescence
250 corresponds to the duration of the growing period.

251 2.4.3 Pattern of the phytoplankton growing period

252 The k-means method (Hartigan and Wong, 1979) is used to characterize the annual patterns of the
253 phytoplankton growing period.
254

255 We exclude the year 2013 from the analysis of the Bay of Vilaine because of a large number of missing
256 data. When the interval over which consecutive data are missing is no longer than one week, we perform a linear
257 interpolation to replace the missing data. A 5-day running average is applied to the Chl-*a* fluorescence signal and
258 data are then normalized by the maximum value. We analyze Chl-*a* fluorescence every year for 150 days after the
259 IPGP.

260 Time series from both bays are merged before application of the k-means and the number of clusters (or
261 centroids) is set at 2 to distinguish the dominant patterns of the phytoplankton growth period at both sites. The use
262 of a larger number of clusters is investigated and does not produce a pattern representing a large number of
263 observed growing periods.

264 2.4.4 Detection of extreme events

265
266 The peak over threshold method (see Oliver *et al.*, 2018 and Poppeschi *et al.*, 2021 for further details) is
267 used to detect hydro-meteorological extreme events such as cold spells, flood events and wind bursts. An event is
268 considered as extreme if values are higher than a given statistical threshold for at least 3 consecutive days. In the
269 present study, the 90-percentile threshold is selected to detect floods and wind bursts, and the 10-percentile to
270 detect cold spells. Seasonal anomalies are calculated over at least 20 years, by subtracting raw data from the winter
271 average value (for cold spells) or from the spring average value (wind bursts and floods).
272
273

274 3. Results

275 3.1 Characterization of the phytoplankton growing period

276
277 The high-frequency *Chl-a* fluorescence time series at both sites show an intense seasonal cycle with low
278 values from November to February and high values from March to October (Fig. 4). Focusing on the period from
279 2010 to 2019 in the Bay of Brest, the minimum *Chl-a* fluorescence is observed during the years 2012 and 2013
280 and does not exceed 7 FFU. In contrast, some years show *Chl-a* fluorescence values above 15 FFU, but can be up
281 to 20 FFU (such as 2010, 2014, 2015 or 2019). In the Bay of Vilaine, a similar seasonal pattern is observed with
282 higher values reaching 50 FFU in 2013. Small (< 20 FFU) and high (> 35 FFU) *Chl-a* fluorescence amplitude are
283 observed occasionally (in 2014 and 2017 and in 2013 and 2016, respectively). The *Chl-a* fluorescence is higher,
284 almost double, in the Bay of Vilaine compared to the Bay of Brest with a mean cumulative *Chl-a* fluorescence
285 around 580 FFU and 360 FFU, respectively (Table 2). The high phytoplankton biomass of the Bay of Vilaine is
286 corroborated by the concentrations measured by low-frequency observation programs (SOMLIT and REPHY).
287

288 The phytoplankton growing period ranges from approximately March 10th to September 30th in both regions
289 (Table 2). The average duration of the phytoplankton growing period is 179 days in the Bay of Vilaine and 200
290 days in the Bay of Brest (Table 2). The phytoplankton growing period is characterized by successive blooms,
291 whose number and intensity are variable from year to year (Fig. 4).
292

293 The main patterns of the phytoplankton growing period are identified by two clusters (Fig. 5). Cluster 0
294 includes the phytoplankton growing period with two successive marked blooms in early spring and in summer,
295 the intensity of the second bloom being highly variable. Cluster 1 is characterized by a plateau during the two first
296 months of the phytoplankton growing period. Most of the patterns of the Bay of Vilaine are in cluster 0 while those
297 of the Bay of Brest are in cluster 1 (Table 3). The years that stand out in the Bay of Brest (2002, 2010, 2014)
298 correspond to years with the highest cumulative *Chl-a* fluorescence (≥ 450 FFU). The atypical years in the Bay
299 of Vilaine (2011, 2017 and 2019) show the lowest cumulative *Chl-a* fluorescence (≤ 450 FFU).

300 3.2 Variability of the Initiation of the Phytoplankton Growing Period (IPGP)

301
302 Calculations performed to determine the IPGP for high- and low-frequency data yield comparable results (Fig.
303 6). The mean differences between the IPGP calculated with the high- and low-frequency data are 5 and 8 days for
304 the Bay of Brest and the Bay of Vilaine, respectively. A difference of only 4 and 6 days between the model
305 simulations (reference year = 2015) and the high-frequency *in situ* data is observed in the Bay of Brest and the
306 Bay of Vilaine, respectively.
307

308 A decadal variability of the IPGP is recorded from mid-February to mid-April in both ecosystems (day 50 to
309 day 102 in the Bay of Brest and day 53 to day 93 in the Bay of Vilaine; Fig. 6). In the Bay of Brest, early IPGPs
310 (day < 53) are observed in 2010 and 2013, whereas late IPGP (day > 93) are observed in 2001, 2017 and 2019. In
311 the Bay of Vilaine, the earliest IPGP is detected in 2012 (day 53) and the latest in 2019 (day 93).
312

313 The variability of IPGP in the Bay of Brest shows two linear trends (Fig. 6a), with a decrease of 52 days from
314 2001 to 2010 (observed in both high- and low-frequency datasets), followed by an increase (+48 days) from 2011
315 to 2019, a decline also observed in the Bay of Vilaine (Fig. 6b). Over the period 2011-2019, the IPGP is shifted
316 towards a later date by +3.5 days per year in the Bay of Vilaine and +3.7 days per year in the Bay of Brest.

317 3.3 Analysis of environmental conditions driving the IPGP

318 3.3.1 Impact of environmental conditions on the IPGP

319
320
321
322
323

We next quantify the influence of environmental drivers on the date of IPGP (Fig. 7). These drivers represent the major limiting factors of the phytoplankton growth and comprise input of nutrients (river flow), PAR (incident light), SST (air temperature, incident light) and turbidity in the water column (river flow, wind intensity, tidal range).

324
325
326
327
328
329
330
331

The median values of the environmental drivers observed at the date of each annual IPGP are very close in both bays (Table 4): temperate SST (10 °C), weak wind (3 m s⁻¹), a medium PAR (1360 W m⁻²), a low turbidity (7 NTU), and a weak tidal amplitude (semi-amplitude of 1.6 m in the Bay of Brest and 0.9 m in the Bay of Vilaine). The IPGP occurs mainly during neap tides at 68% in the Bay of Brest and 77% in the Bay of Vilaine. The river flow is low during the IPGP with a runoff of 46 m³ s⁻¹ for the Aulne, 96 m³ s⁻¹ for the Vilaine, and 1196 m³ s⁻¹ for the Loire. These values are considered to be the favorable environmental conditions for this study.

332
333
334
335
336

To assess how environmental drivers may impact (i.e. advance or delay) the IPGP, we focus on the 15 days before the mean day of the IPGP (day 68) and of each annual IPGP. The considered 15 days length is related to the typical water residence time in both bays (Frere *et al.*, 2017; Poppeschi *et al.*, 2021 for the Bay of Brest - Chapelle *et al.*, 1994; Ratmaya *et al.*, 2019 for the Bay of Vilaine).

337
338
339
340
341

The earliest IPGP dates (IPGP < day 55) are associated with earlier occurrence of favorable environmental conditions than the other years. Earliest IPGP in 2010 and 2013 in the Bay of Brest and in 2012 in the Bay of Vilaine occurred before day 55 (Fig. S1f, 7c - S2a). Early IPGP between day 55 to 60, also associated with favorable environmental conditions, are found in 2002 and 2016 in the Bay of Brest (Fig. S1b, S1j).

342
343
344
345
346
347
348

The latest IPGP dates (IPGP > day 90) are associated with unfavorable environmental conditions until the date of the IPGP. Latest IPGP occurring after day 90 are observed in 2001, 2003, 2017 and 2019 in the Bay of Brest and in 2019 in the Bay of Vilaine (Fig. S1a,c,k,l - S2g). For example, the delay detected in 2017 in both bays is due to strong wind and a lack of PAR until the day of IPGP (Fig. S1k - Fig. S2e). Late IPGP between day 70 to 90 are recorded in 2004, 2007 and 2012 in the Bay of Brest, and in 2014, 2017 and 2018 in the Bay of Vilaine (Fig. S1d,e,g, 7d - S2e,f).

349
350
351
352
353
354

The interannual variability of the date of the IPGP is therefore not controlled by a unique environmental driver. When the values of the environmental drivers responsible for the IPGP (Table 4) are compared to the mean values of the environmental drivers over a period of 30 days around the IPGP (Table S1), threshold values are observed in both bays: river flow is lower than usual (between 10 and 30 m³ s⁻¹), temperature is close to the expected value (10 °C), wind is weak (0.5 to 1.5 m s⁻¹), PAR is stronger (>300 W m⁻²), and turbidity is low (about 1.5 NTU). IPGP starts around day 68 (±3 days) on average (Fig. 7a,b).

355 3.3.2 Modeling the importance of the environmental drivers

356
357
358

The relative contribution of each environmental driver on the IPGP is determined by MARS-1DV simulations starting on February 1st (Fig. 8). Environmental drivers tested in the model are controlling:

359
360
361
362

- sea temperature - explored in the model through air temperature (SST proxy),
- the level of water turbulence - through wind intensity,
- the available light - controlled by Cloud Coverage (CC, as a sea surface PAR proxy) and the erosion rate (turbidity proxy) limiting light penetration in the water column.

363
364
365
366
367
368

Model results show that early IPGP are associated with air temperature higher than 9 °C (resulting in SST higher than 8 °C), low wind intensity, weak CC and low erosion rate. Environmental drivers responsible for early or late IPGP are similar in both bays. Air temperature is the main driver with a potential deviation from the mean IPGP of 25 days in the Bay of Brest and 40 days in the Bay of Vilaine (Fig. 8). Wind, CC and erosion rate have a lower impact on the IPGP (around 6 days in the Bay of Brest and 13 days in the Bay of Vilaine). In the Bay of Vilaine, the environmental drivers can simulate later IPGP than in the Bay of Brest.

369 In the Bay of Brest (Fig. 8a), only variations in air temperature have a real impact on the IPGP. If air
370 temperature is low ($< 8^{\circ}\text{C}$), the IPGP is not triggered before day 74 (Table 5, Exp 1). If air temperature is high
371 ($>13^{\circ}\text{C}$), the IPGP can start on day 49 (Table 5, Exp 2).
372

373 In the Bay of Vilaine, air temperature and the erosion rate are the two main drivers impacting the IPGP (Fig.
374 8b). As in the Bay of Brest, if air temperature is low ($< 6^{\circ}\text{C}$), the IPGP is late and appears only after day 80 (Table
375 5, Exp 1). If temperature is equal or above 13°C , the IPGP is early and appears on day 45 (Table 5, Exp 2). If the
376 erosion rate is low ($2 \cdot 10^{-7} \text{ kg m}^{-2} \text{ s}^{-1}$), the IPGP takes place on day 76 (Table 5, Exp 7). If the erosion rate is high
377 ($2 \cdot 10^{-5} \text{ kg m}^{-2} \text{ s}^{-1}$), the IPGP occurs late after day 87 (Table 5, Exp 8).
378

379 Even if variations in wind and CC induce weaker shifts in the date of the IPGP, i.e. about one week at the
380 most (Table 5, Exp 3,4,5,6), they can however explain some variations in IPGP. For example, the fact that the
381 early IPGPs, observed in 2010 in the Bay of Brest and in 2012 in the Bay of Vilaine, are due to low wind conditions
382 (around 2 m s^{-1} , Fig. S2a - S1f) are confirmed by both *in situ* measurements and the model (Fig. 8b).
383

384 The combined effect of the environmental factors can also be explored from the MARS-1DV model
385 simulations (Fig. 9). The modeling conditions (hereafter called “Exp”) are detailed in Table 5 and compared to the
386 mean IPGP date (day 68).
387

388 The simulations confirm the observations, late IPGP correspond to the most extreme unfavorable
389 combined environmental values (temperature of 4°C , wind intensity of 10 m s^{-1} , CC of 100% and erosion rate of
390 $2 \cdot 10^{-5} \text{ kg m}^{-2} \text{ s}^{-1}$ - Exp A). **Due to the most unfavorable conditions, the IPGP occurs 9 days and 64 days later in the**
391 **Bay of Brest and in the Bay of Vilaine, respectively.** Late IPGP can also be linked to the combined effect of only
392 two factors such as: “temperature and wind” and “temperature and CC” with a delay of 5 and around 22 days
393 respectively (Exp B and C). In contrast, no delay is observed for the combination “wind and CC” (Exp D) in both
394 bays.
395

396 Early IPGP events are found in the model simulations and in the *in situ* observations when conditions
397 correspond to a high temperature (14°C), no wind intensity and CC, and a low erosion rate ($2 \cdot 10^{-7} \text{ kg m}^{-2} \text{ s}^{-1}$) -
398 Exp K. All the combined scenarios allow the occurrence of an earlier IPGP (by at least 5 additional days) compared
399 to experiments that consider a single modified parameter.
400

401 This analysis enables environmental parameters to be classified with respect to their impact on the IPGP.
402 In both bays, the temperature appears to be the key factor driving the IPGP. By combining the environmental
403 drivers, the IPGP can occur even later or earlier than with a single forcing. In both bays, the combination of wind
404 and CC has no impact on the IPGP, which occurs near the median day (Exp D and N). The extreme couplings of
405 Exp A,E,F,G,J delay the date of IPGP later than detected in the observations for the Bay of Vilaine. All simulations
406 show a higher impact on the date of IPGP in the Bay of Vilaine than in the Bay of Brest (Fig. 9, Table 5).

407 3.4 Impact of extreme hydro-meteorological events on the IPGP

408 3.4.1 Cold spells

409 The impact of cold spells on the IPGP is simulated with the MARS-1DV model based on two criteria: (i)
410 the period of occurrence of the event, set in mid- or end February, (ii) the duration and intensity of the cold spell,
411 which can be either short and weak (8 days, 7°C) or long and intense (20 days, 5°C) (Fig. 10).

412 In both bays, when the cold spell appears in mid-February, the IPGP is not impacted. However, it is
413 delayed by about 15 days when occurring at the end of February. The duration of the cold spell, when longer than
414 15 days, also has an impact on the IPGP, with a delay of 13 and 12 days in the Bay of Brest and in the Bay of
415 Vilaine, respectively.

416 Eight cold spells are detected in February in both bays between 2001 and 2019. In 2011, both sites are
417 impacted simultaneously with cold spells. Long cold spells (30 days) are observed in 2009 and 2018, leading to
418 an anomaly of more than -1.9°C .

419 The cold spell observed in 2018 in the Bay of Vilaine may explain the later IPGP. There is no change in
420 the IPGP in 2011 and 2013, despite the cold spell, the period of occurrence being too early during winter 2011,
421 and the duration too short in 2013 (only 10 days).

422 In the Bay of Brest, the cold spells in 2003 and 2004 may explain the delay of the IPGP (respectively
423 days 93 and 85). The presence of long and intense cold spells in 2010 and 2011 do not shift the IPGP (days 50 and
424 67) because they occur too early (before day 20).

425 3.4.2 Wind bursts

426 Based on our model simulations, the wind bursts that occur during at least three continuous days have no
427 impact on the IPGP in both bays, whatever the duration, the period and the intensity (± 1 day). In the Bay of
428 Vilaine, only one wind event is detected in 2018 (3 days long and 6 m s^{-1}). In the Bay of Brest, several events are
429 detected, but no significant impact is observed on the IPGP.
430
431

432 3.4.3 Flood events

433 River floods can delay the IPGP by resuspending sediment in the water column and therefore limiting
434 light penetration in the water column. Inputs of nutrients have no impact during the late winter period because
435 nutrient concentrations are maximal, with no limitation on phytoplankton growth. Flood events are analyzed with
436 observation data collected in the month prior to the IPGP date because the 1DV modeling approach does not allow
437 the sensitivity to hydrological events to be simulated (*i.e.* it is necessary to simulate horizontal advection
438 processes).
439

440 In the Bay of Brest, the impact of flood events depends on their duration and intensity: when the flood
441 exceeds 15 days, a delay in the IPGP is detected. Shorter and more intense floods ($> 300 \text{ m}^3 \text{ s}^{-1}$) do not impact the
442 IPGP.
443

444 In the Bay of Vilaine, only two flood events are observed close to the IPGP date in 2014 and 2015. The
445 2015 flood event, which is 10 days longer and more intense ($> 100 \text{ m}^3 \text{ s}^{-1}$) than the 2014 one, delays the IPGP date
446 by 10 days.
447
448

449 4 Discussion

450 4.1 Comparison of the phytoplankton growing period in both bays

451 Despite their contrasting hydrodynamics (*e.g.* Petton *et al.*, 2020; Poppeschi *et al.*, 2021; Lazure and
452 Jegou, 1998; Ratmaya *et al.*, 2019; Menesguen *et al.*, 2019), the median dates of the start and the end of the
453 phytoplankton growing period are the same in the Bay of Brest and in the Bay of Vilaine, whether they are
454 calculated from high- and low- frequency datasets or model simulations. The phytoplankton growing period occurs
455 from March to September and lasts about 190 days in both bays. This concordance is related to a similar seasonality
456 of the environmental drivers.
457
458

459 The observed cumulative fluorescence is almost double in the Bay of Vilaine compared with the Bay of
460 Brest. This difference in the amount of chlorophyll produced in surface waters from both bays is also recorded by
461 the low-frequency observation programs and satellite observations (Menesguen *et al.*, 2019). It can be explained
462 by the difference of the hydrodynamics and the influence of different watersheds. The Bay of Brest is a semi-
463 enclosed bay with a macro-tidal regime influenced by two local rivers (Aulne and Elorn), whereas the Bay of
464 Vilaine has a weaker tidal regime, is open on the continental shelf and is widely influenced by a large river (Loire
465 river).
466
467

468 Two different patterns of the phytoplankton growing period are identified by the k-means classification
469 in both bays. The flattened, weak and long bloom highlighted in the Bay of Brest can be explained by assuming
470 that nutrients are not limiting the phytoplankton growth during spring. The maintenance of the diatom succession
471 throughout spring since the 1980s (Quéguiner 1982; Del Amo *et al.*, 1997) can be explained by the combination
472 of increasing N and P loads, intense Si recycling and a macrotidal regime (Ragueneau *et al.*, 2019). The
473 phytoplankton growing period in the Bay of Vilaine is characterized by several successive peaks including two
474 main ones. Nutrients drive the seasonal evolution of the phytoplankton growing period through periods of nutrient-
475 limited conditions. These fluctuations are governed by phosphorus and nitrate loads from Vilaine and Loire rivers

476 (Ratmaya *et al.*, 2019), but probably also by the stoichiometry of recycled elements in the water and at the water-
477 sediment interface (Ratmaya *et al.*, 2022). At the beginning of the phytoplankton growing period (IPGP), however,
478 the system is not nutrient-limited in terms of nitrate, phosphorus and silicate (Table 4).
479

480 4.2 Validation of the method for IPGP detection

481
482 The method that we developed to detect IPGP on both high-frequency and low-frequency *in situ*
483 observations shows comparable results and detects similar initiation dates for some years, while a time lag between
484 high- and low-frequency observations can be observed for other years. This difference is mainly explained by the
485 difference in the sampling frequency. The late deployment of the buoy in the Bay of Vilaine (i.e. not deployed
486 until mid-February before 2018) can also explain some differences between both sites. High-frequency data
487 provide a more accurate detection of the day of the IPGP, while an uncertainty of about ± 7 days is observed with
488 low-frequency observations. This comparison between high- and low-frequency based IPGP detection highlights
489 the sensitivity of sampling strategy in the observation of phytoplankton growing periods (Bouman *et al.*, 2005;
490 Serre-Fredj *et al.*, 2021) related to the response of the ecosystem within a few hours after an environmental change
491 (Lefort and Gasol, 2014; Thyssen *et al.*, 2008).
492

493 The modeled IPGP, based on the year 2015, is coherent with high-frequency observations (around 5 days
494 of difference between modeled and observed IPGP). Considering the idealized framework for modeling
495 computations (1DV model instead of a realistic 3D model configuration), the agreement between observations and
496 simulations validates the 1DV approach to explore IPGP dynamics. With the 1DV configuration, the vertical
497 dynamics in the water column, coupled with biogeochemistry and sediment dynamics are well reproduced.
498 Atmospheric forcings and interactions with the bottom layer are the main environmental drivers. The full range of
499 impacts related to the horizontal advection (*e.g.* in considered regions, rivers advected plumes can change the
500 hydrodynamics and the nutrient fluxes) are not evaluated, however. In the Bay of Brest and in the Bay of Vilaine,
501 such advected sources exist (Poppeschi *et al.*, 2021; Lazure and Jegou, 1998). But inputs from rivers are not main
502 drivers of the IPGP in nutrient-rich environments. Nutrient loads advected by rivers may impact the phytoplankton
503 community later during the growing period rather than at IPGP (Ratmaya *et al.*, 2019).
504

505 4.3 Identification of the environmental conditions supporting the IPGP

506
507 The main theories to explain the initiation of phytoplankton blooms (Sverdrup, 1953; Huisman *et al.*,
508 1999; Banse, 1994) are not relevant in the context of shallow and well-mixed coastal waters under the influence
509 of river plumes. In the studied region, the ecosystem does not evolve with mixed layer dynamics, as observed in
510 deeper environments. Both bays are permanently vertically mixed mainly by tides, and vertical stratification only
511 occurs on a thin surface layer due to river runoffs at short time scales. However, the IPGP is mainly driven and
512 limited by similar local environmental conditions in both bays. The ideal temperature (> 10 °C) and PAR (1300
513 $W m^{-2}$) for the IPGP are in agreement with those from previous studies conducted in similar coastal ecosystems
514 (*e.g.* Glé *et al.*, 2007; Townsend *et al.*, 1994; Trombetta *et al.*, 2019). Neap tidal conditions, weak wind (lower
515 than $3 m s^{-1}$) and weak river flow can also play a positive role to observe earlier IPGP according to the previous
516 studies (Ragueneau *et al.*, 1996; Tian *et al.*, 2011). The impact of wind direction on the IPGP is negligible.
517 Local changes in temperature, incident radiation, tidal conditions, wind conditions and river flow, induce
518 differences in detected IPGP. In this coastal temperate ecosystem, we observe that the beginning of the growing
519 period is limited by light (controlled by incident radiation, turbidity at this season), and water temperature. The
520 IPGP also occurs during low vertical mixing conditions.
521

522 The comparison of the individual importance of each environmental driver shows that temperature and
523 light penetration are the key environmental drivers in both bays. When light penetration is reduced by a combined
524 effect of PAR and turbidity (sediment resuspension), the delay of IPGP can be amplified, especially in the Bay of
525 Vilaine. The importance of light availability in the timing and intensity of the spring bloom is also highlighted in
526 the North Sea (Wiltshire *et al.*, 2015), in the German Bight (Tian *et al.*, 2009) and along the UK South Coast
527 (Iriarte and Purdie, 2004).
528

529 4.4 Interannual evolutions of the IPGP

530
531 The IPGP in these two bays shows a strong interannual variability with initiation dates varying from late
532 winter to spring, depending on the environmental conditions. A mean difference of 50 days between the earliest
533 and latest IPGP dates is observed. It is important to note that the phytoplankton population during the IPGP is
534 always dominated in both bays by the same centric diatoms, genera *Chaetoceros* and *Skeletonema*, whose

535 abundance varies from year to year depending on climatic conditions (REPHY, 2021). None of the nutrient is
536 limiting the growing of phytoplankton at the IPGP (Table 4).

537
538 The earliest IPGP are observed and related to favorable environmental conditions early in the year. For
539 example, the IPGP can occur before day 50, associated with exceptionally weak wind and river flow in addition
540 to a sufficient PAR and nearly-optimal temperature of around 10 °C (e.g. 2010 in the Bay of Brest and 2012 in the
541 Bay of Vilaine). But if the environmental conditions are not favorable (e.g. 2017 and 2019 in both bays), the IPGP
542 is delayed. This can be due to: 1- strong wind during several days (not a single wind burst) combined with a weak
543 PAR and enhanced sometimes by high turbidity events which further limits the light penetration. 2- low SST.

544
545 The IPGP appears to be more controlled by local environmental drivers than by regional environmental
546 drivers, the IPGP being earlier in one site than in the other during half of the studied years: for example, the 2012
547 IPGP is early in the Bay of Vilaine (day 53), but late in the Bay of Brest (day 80), related to strong wind activity
548 and low PAR on the last bay. The offshore regional dynamics will induce limited impacts on local hydrodynamical
549 features that will change IPGP.

550
551 Changes in the IPGP over the last two decades has highlighted its evolution through two trends: it occurs
552 earlier each year until 2010, when the trend is reversed. Changes in environmental conditions over the last 20 years
553 was then studied to seek a possible concordance with one of the environmental drivers, but no significant trend
554 was detected. Because of global warming, earlier phytoplankton blooms are expected (Friedland *et al.*, 2018) but
555 not later IPGP as observed in our study regions. However, the mechanisms that trigger blooms in coastal
556 ecosystems - especially eutrophic ones - are not similar to the processes that influence blooms in the open ocean.
557 No link between trends in IPGP and environmental drivers has not been identified in the southern California Bight
558 from 1983 to 2000 (Kim *et al.*, 2009). By investigating long-term (1975-2005) daily data, Wiltshire *et al.* (2008)
559 also observe later phytoplankton blooms in the German bight, but no link to global warming was detected. Henson
560 *et al.* (2018) model a bloom shift of 5 days per decade from 2006 to 2025, with later blooms. A possible explanation
561 of these later IPGP may involve a lower spring SST (Hunter-Cervera *et al.*, 2016).

562 4.5 Extreme events

563
564 We show that a cold spell is likely to delay the IPGP if it occurs at the end of winter (after 20th February)
565 or/and if the cold spell lasts long enough (> 15 days). The drop in temperature related to the cold spell prevents
566 the IPGP in both bays. This is in accordance with the study of Gomez and Souissi (2008) in the English Channel
567 where cold spells can delay the date of IPGP, as a result of an increase in water column mixing. Cold spells may
568 also drive local patterns by influencing the phytoplankton communities (Gomez and Souissi, 2008; Schlegel *et al.*,
569 2021).

570
571 Flood events have an influence on the phytoplankton biomass when they occur in spring, due to the supply
572 of nutrients. When they occur in late winter, nutrients are already at their maximum. The impact of floods on IPGP
573 is then due to the increase of the water turbulence and to the limitation of light by increasing the turbidity. The
574 IPGP can be delay only if floods are at least 15 days long. This scheme was also observed by Saeck *et al.* (2013)
575 along a river-estuary-bay continuum and explained by a shortened water residence time and limited-light due to
576 flood-induced turbidity in the coastal zone.

577
578 No relationship is observed between wind events and IPGP in both bays because they are weakly
579 stratified, contrary to open seas (*i.e.* Black Sea, Mikaelyan *et al.*, 2017). In coastal stratified regions (e.g. under
580 the influence of river plumes), strong wind and tidal mixing can enhance the mixing and break down stratification,
581 which **does not favor phytoplankton growth** (Joordens *et al.*, 2021). During the IPGP, except during floods, both
582 regions are weakly stratified and are then less sensitive to combined wind/tidal short events.

583 **584**

585 **5 Conclusions**

586
587 This study provides a new understanding of the IPGP dynamics in coastal temperate areas by using both
588 high and low-frequency *in situ* data, in combination with simulations from a 1DV model. Strong similarities are
589 found in both bays. An important interannual variability of the IPGP is observed, with a trend towards a later IPGP
590 over the last decade (2010-2020). We quantify the importance of environmental conditions on the IPGP. When
591 we compare observed IPGP with favorable environmental conditions and following sensitivity experiments with
592 the 1DV model, water temperature and turbidity (limiting light penetration in the water column) appear as the

593 main drivers explaining interannual IPGP variability. The IPGP is a complex mechanism, usually triggered by
594 more than one environmental parameter. The analysis of the influence of extreme events reveals that cold spells
595 and floods have a strong impact by delaying the IPGP when episodes are long enough and occur after winter. No
596 effect of wind bursts is detected.

597 While this study shows comparable IPGP dynamics when based on 1DV model simulations or *in situ*
598 observations, we will next investigate the effect on phytoplankton dynamics of a fully realistic hydrodynamics
599 (including horizontal and vertical advections; mixing processes; remote sources of nutrients from rivers) 3D
600 model. We will focus on exploring the variability of phytoplankton communities during IPGP to assess whether
601 community change is occurring, as observed in other studies and for other ecosystems (Ianson *et al.*, 2001;
602 Edwards and Richardson, 2004; Chivers *et al.*, 2020). When interannual evolutions in the phytoplankton growth
603 are explored, the detection and the understanding of harmful algal bloom dynamics can also be addressed based
604 on similar approaches. Further studies will be dedicated to the simulation of the coastal ecosystem in the future
605 based on numerical simulation through climate scenarios. The investigation of other contrasting coastal
606 environments will allow us to better understand and anticipate the expected impact of global change on coastal
607 phytoplankton dynamics.

608 **Author contributions**

609 CP, GC, AD, RV, PR-M and EGo conceptualized the study. PR-M, EGr and MR collected data. MP and GC
610 developed the model configuration. CP, GC, AD and RV drafted the first versions of the paper. CP carried out all
611 the analyses and wrote the final version of the paper. All authors contributed to the discussions and revisions of
612 the study.

613 **Acknowledgements**

614 We would like to acknowledge COAST-HF (<http://www.coast-hf.fr>), SOMLIT ([http://somalit.epoc.u-](http://somalit.epoc.u-bordeaux1.fr)
615 [bordeaux1.fr](http://somalit.epoc.u-bordeaux1.fr)) and REPHY (<https://doi.org/10.17882/47248>) national observing networks, for providing data flux
616 readily available. COAST-HF and SOMLIT are components of the National Research Infrastructure ILICO. We
617 would like to thank the Shom for tidal data and also Météo-France for wind and solar flux products. We also thank
618 Dr Claire Labry for fruitful discussions and Dr Sally Close for her proofreading. We thank the referees for their
619 helpful and constructive comments.

620 **Financial support**

621 This study is part of the State-Region Plan Contract ROEC supported in part by the European Regional
622 Development Funds and the COXTCLIM project funded by the Loire-Brittany Water Agency, the Brittany region
623 and Ifremer.

624 **References**

- 625 Aminot, A., and Kerouel, R.: Hydrologie des écosystèmes marins. Paramètres et analyses, Editions de l'Ifremer,
626 336 p., ISBN 2-84433-133-5, 2004.
- 627
- 628 Banse, K.: Grazing and zooplankton production as key controls of phytoplankton production in the open
629 ocean, *Oceanography*, 7(1), 13-20, <https://www.jstor.org/stable/43925524>, 1994.
- 630 Barbosa, A., Domingues, R., and Galvão., H.: Environmental forcing of phytoplankton in a Mediterranean estuary
631 (Guadiana estuary, south-western Iberia): A decadal study of anthropogenic and climatic influences, *Estuaries and*
632 *Coasts*, doi:10.1007/ s12237-009-9200-x, 2010.
- 633 Bedford, J., Ostle, C., Johns, D. G., Atkinson, A., Best, M., Bresnan, E., ... and McQuatters-Gollop, A.: Lifeform
634 indicators reveal large-scale shifts in plankton across the North-West European shelf, *Global Change Biology*,
635 26(6), 3482-3497, doi:10.1111/gcb.15066, 2020.
- 636 Behrenfeld, M. J.: Abandoning Sverdrup's critical depth hypothesis on phytoplankton blooms, *Ecology*, 91(4),
637 977-989, doi:10.1890/09-1207, 2010.

638
639 Behrenfeld, M. J., Doney, S. C., Lima, I., Boss, E. S., and Siegel, D. A.: Annual cycles of ecological disturbance
640 and recovery underlying the subarctic Atlantic spring plankton bloom, *Global biogeochemical cycles*, 27(2), 526-
641 540, doi:10.1002/gbc.20050, 2013.

642
643 Beucher, C., Treguer, P., Corvaisier, R., Hapette, A. M., and Elskens, M.: Production and dissolution of biosilica,
644 and changing microphytoplankton dominance in the Bay of Brest (France), *Marine Ecology Progress Series*, 267,
645 57-69, doi:10.3354/meps267057, 2004.

646
647 Boss, E., and Behrenfeld, M.: In situ evaluation of the initiation of the North Atlantic phytoplankton bloom,
648 *Geophysical Research Letters*, 37(18), doi:10.1029/2010GL044174, 2010.

649
650 Bouman, H., Platt, T., Sathyendranath, S., and Stuart, V.: Dependence of light-saturated photosynthesis on
651 temperature and community structure, *Deep Sea Research Part I: Oceanographic Research Papers*, 52(7), 1284-
652 1299, doi:10.1016/j.dsr.2005.01.008, 2005.

653
654 Brody, S. R., Lozier, M. S., and Dunne, J. P.: A comparison of methods to determine phytoplankton bloom
655 initiation, *Journal of Geophysical Research, Oceans*, 118(5), 2345-2357, doi:10.1002/jgrc.20167, 2013.

656
657 Caracciolo, M., Beaugrand, G., Hélaouët, P., Gevaert, F., Edwards, M., Lizon, F., ... and Goberville, E.: Annual
658 phytoplankton succession results from niche-environment interaction, *Journal of Plankton Research*, 43(1), 85-
659 102, doi:10.1093/plankt/fbaa060, 2021.

660
661 Chapelle, A., Lazure, P., and Ménesguen, A.: Modelling eutrophication events in a coastal ecosystem. Sensitivity
662 analysis, *Estuarine, Coastal and Shelf Science*, 39(6), 529-548, doi:10.1016/S0272-7714(06)80008-9, 1994.

663
664 Charria, G., Lazure, P., Le Cann, B., Serpette, A., Reverdin, G., Louazel, S., Batifoulier, F., Dumas, F., Pichon,
665 A. and Morel, Y. Surface layer circulation derived from Lagrangian drifters in the Bay of Biscay. *Journal of*
666 *Marine Systems*, 109, 60-76, doi:10.1016/j.jmarsys.2011.09.015, 2013.

667
668 Chiswell, S. Calil, P. and Boyd, P. Spring blooms and annual cycles of phytoplankton: a unified
669 perspective. *Journal of Plankton Research*, 37(3), 500-508, doi:10.1093/plankt/fbv021, 2015.

670
671 Chivers, W. J., Edwards, M., and Hays, G. C.: Phenological shuffling of major marine phytoplankton groups over
672 the last six decades, *Diversity and Distributions*, 26(5), 536-548, doi:10.1111/ddi.13028, 2020.

673
674 Cloern, J. E.: Phytoplankton bloom dynamics in coastal ecosystems: a review with some general lessons from
675 sustained investigation of San Francisco Bay, California, *Reviews of Geophysics*, 34(2), 127-168,
676 doi:10.1029/96RG00986, 1996.

677
678 Cocquempot, L., Delacourt, C., Paillet, J., Riou, P., Aucan, J., Castelle, B., Charria, G., Claudet, J., Conan, P.,
679 Coppola, L., Hocdé, R., Planes, S., Raimbault, P., Savoye, N., Testut, L., and Vuillemin, R.: Coastal Ocean and
680 Nearshore Observation: A French Case Study, *Frontiers in Marine Science*, 6(324), 1-17,
681 doi:10.3389/fmars.2019.00324, 2019.

682
683 Cook, P. L., Holland, D. P., and Longmore, A. R.: Effect of a flood event on the dynamics of phytoplankton and
684 biogeochemistry in a large temperate Australian lagoon, *Limnology and Oceanography*, 55(3), 1123-1133,
685 doi:10.4319/lo.2010.55.3.1123, 2010.

686
687 Cugier, P., Billen, G., Guillaud, J. F., Garnier, J., and Ménesguen, A.: Modelling the eutrophication of the Seine
688 Bight (France) under historical, present and future riverine nutrient loading, *Journal of Hydrology*, 304(1-4), 381-
689 396, doi:10.1016/j.jhydrol.2004.07.049, 2005.

690
691 Del Amo, Y., Le Pape, O., Tréguer, P., Quéguiner, B., Ménesguen, A., and Aminot, A.: Impacts of high-nitrate
692 freshwater inputs on macrotidal ecosystems. I. Seasonal evolution of nutrient limitation for the diatom-dominated
693 phytoplankton of the Bay of Brest (France), *Marine Ecology Progress Series*, 161, 213-224, doi:10.5194/bg-16-
694 1361-2019, 1997.

695

696 Edwards, M., and Richardson, A. J.: Impact of climate change on marine pelagic phenology and trophic
697 mismatch, *Nature*, 430(7002), 881-884, doi:10.1038/nature02808, 2004.
698

699 Farcy, P., Durand, D., Charria, G., Painting, S.J., Tamminem, T., Collingridge, K., Grémare, A.J., Delauney, L.,
700 and Puillat, I.: Toward a European coastal observing network to provide better answers to science and to societal
701 challenges; the JERICO research infrastructure, *Frontiers in Marine Science*, 6, 1–13,
702 doi:10.3389/fmars.2019.00529, 2019.
703

704 Ferrer, L., Fontán, A., Mader, J., Chust, G., González, M., Valencia, V., Uriarte, Ad. and Collins, M.B. Low-
705 salinity plumes in the oceanic region of the Basque Country. *Continental Shelf Research* 29 (8), 970–984,
706 doi:10.1016/j.csr.2008.12.014, 2009.
707

708 Frère, L., Paul-Pont, I., Rinnert, E., Petton, S., Jaffré, J., Bihannic, I., Soudant, P., Lambert, C. and Huvet, A.:
709 Influence of environmental and anthropogenic factors on the composition, concentration and spatial distribution
710 of microplastics : a case study of the Bay of Brest (Brittany, France), *Environ. Pollut*, 225, 211–222,
711 doi:10.1016/j.envpol.2017.03.023, 2017.
712

713 Friedland, K. D., Mouw, C. B., Asch, R. G., Ferreira, A. S. A., Henson, S., Hyde, K. J., ... and Brady, D. C.:
714 Phenology and time series trends of the dominant seasonal phytoplankton bloom across global scales, *Global
715 Ecology and Biogeography*, 27(5), 551-569, doi:10.1111/geb.12717, 2018.
716

717 Glé, C., Del Amo, Y., Bec, B., Sautour, B., Froidefond, J. M., Gohin, F., Maurer, D., Plus, M., Laborde, P., and
718 Chardy, P.: Typology of environmental conditions at the onset of winter phytoplankton blooms in a shallow
719 macrotidal coastal ecosystem, Arcachon Bay (France), *Journal of plankton research*, 29(11), 999-1014,
720 doi:10.1093/plankt/fbm074, 2007.
721

722 Gohin, F., Van der Zande, D., Tilstone, G., Eleveld, M. A., Lefebvre, A., Andrieux-Loyer, F., Blauw, A. N.,
723 Bryère, P., Devreker, D., Garnesson, P., Hernández Fariñas, T., Lamaury, Y., Lampert, L., Lavigne, H., Menet-
724 Nedelec, F., Pardo, S., and Saulquin, B.: Twenty years of satellite and in situ observations of surface chlorophyll-
725 a from the northern Bay of Biscay to the eastern English Channel. Is the water quality improving ? *Remote Sensing
726 of Environment*, 233(September), 111343, doi:10.1016/j.rse.2019.111343, 2019.
727

728 Gomez, F., and Souissi, S.: The impact of the 2003 heat wave and the 2005 cold wave on the phytoplankton in the
729 north-eastern English Channel, *Comptes Rendues Biologies*, 331(9), 678-685, doi:10.1016/j.crv.2008.06.005,
730 2008.

731 Grasso F., Le Hir P., and Bassoullet P.: Numerical modelling of mixed-sediment consolidation, *Ocean Dynamics*,
732 65(4), 607– 616, doi:10.1007/s10236-015-0818-x, 2015.

733 Hartigan, J., and Wong, M.: Algorithm AS 136: A K-Means Clustering Algorithm. *Journal of the Royal Statistical
734 Society, Series C (Applied Statistics)*, 28:1, 100-108, doi:2346830, 1979.
735

736 Henson, S. A., Cole, H. S., Hopkins, J., Martin, A. P., and Yool, A.: Detection of climate change-driven trends in
737 phytoplankton phenology, *Global Change Biology*, 24(1), e101-e111, doi:10.1111/gcb.13886, 2018.
738

739 Huisman, J. E. F., van Oostveen, P., and Weissing, F. J.: Critical depth and critical turbulence: two different
740 mechanisms for the development of phytoplankton blooms, *Limnology and oceanography*, 44(7), 1781-1787,
741 doi.org/10.4319/lo.1999.44.7.1781, 1999.
742

743 Hunter-Cevera, K. R., Neubert, M. G., Olson, R. J., Solow, A. R., Shalapyonok, A., and Sosik, H. M.:
744 Physiological and ecological drivers of early spring blooms of a coastal phytoplankter, *Science*, 354(6310), 326-
745 329, doi:10.1126/science.aaf8536, 2016.
746

747 Husson, B., Hernández-Fariñas, T., Le Gendre, R., Schapira, M., and Chapelle, A.: Two decades of Pseudo-
748 nitzschia spp. blooms and king scallop (*Pecten maximus*) contamination by domoic acid along the French Atlantic
749 and English Channel coasts: Seasonal dynamics, spatial heterogeneity and interannual variability, *Harmful
750 Algae*, 51, 26-39, doi:10.1016/j.hal.2015.10.017, 2016.
751

752 Ianson, D., Pond, S., and Parsons, T.: The spring phytoplankton bloom in the coastal temperate ocean: growth
753 criteria and seeding from shallow embayments, *Journal of oceanography*, 57(6), 723-734,
754 doi.org/10.1023/A:1021288510407, 2001.

755
756 IPCC: Summary for Policymakers. In: *Climate Change 2021: The Physical Science Basis. Contribution of*
757 *Working Group I to the Sixth Assessment Report of the Intergovernmental Panel on Climate Change* [Masson-
758 Delmotte, V., P. Zhai, A. Pirani, S. L. Connors, C. Péan, S. Berger, N. Caud, Y. Chen, L. Goldfarb, M. I. Gomis,
759 M. Huang, K. Leitzell, E. Lonnoy, J.B.R. Matthews, T. K. Maycock, T. Waterfield, O. Yelekçi, R. Yu and B. Zhou
760 (eds.)], Cambridge University Press, In Press, 2021.

761
762 Iriarte, A., and Purdie, D. A.: Factors controlling the timing of major spring bloom events in an UK south coast
763 estuary, *Estuarine, Coastal and Shelf Science*, 61(4), 679-690, doi:10.1016/j.ecss.2004.08.002, 2004.

764
765 Isemer, H.-J. and Hasse, L. The Bunker Climate Atlas of the North Atlantic Ocean, 2 Vols. Springer, Berlin. 218-
766 252, 1985.

767
768 Joordens, J. C. A., Souza, A. J., & Visser, A.: The influence of tidal straining and wind on suspended matter and
769 phytoplankton distribution in the Rhine outflow region. *Continental Shelf Research*, 21(3), 301-325,
770 doi:10.1016/S0278-4343(00)00095-9, 2001.

771
772 Kromkamp, J. C., and Van Engeland, T.: Changes in phytoplankton biomass in the western Scheldt estuary during
773 the period 1978-2006, *Estuaries and Coasts*, 33(2), 270–285, doi:10.1007/s12237-009-9215-3, 2010.

774
775 Kim, H. J., Miller, A. J., McGowan, J., and Carter, M. L.: Coastal phytoplankton blooms in the Southern California
776 Bight, *Progress in Oceanography*, 52(2), 137-147, doi:10.1016/j.pocean.2009.05.002, 2009.

777
778 Lazure, P., Jégou, A.-M. and Kerdreux, M. Analysis of salinity measurements near islands on the French
779 continental shelf of the Bay of Biscay. *Scientia Marina* 70 (S1), 7–14, 2006.

780
781 Lazure, P., and Dumas, F.: An external–internal mode coupling for a 3D hydrodynamical model for applications
782 at regional scale (MARS), *Advances in water resources*, 31(2), 233-250, doi:10.1016/j.advwatres.2007.06.010,
783 2008.

784
785 Lazure, P., and Jégou, A. M.: 3D modelling of seasonal evolution of Loire and Gironde plumes on Biscay Bay
786 continental shelf, *Oceanologica acta*, 21(2), 165-177, doi:10.1016/S0399-1784(98)80006-6, 1998.

787
788 Le Boyer, A., Charria, G., Le Cann, B., Lazure, P., and Marié, L. Circulation on the shelf and the upper slope of
789 the Bay of Biscay. *Continental Shelf Research*, 55, 97-107, doi:10.1016/j.csr.2013.01.006, 2013.

790
791 Lefort, T., and Gasol, J. M.: Short-time scale coupling of picoplankton community structure and single-cell
792 heterotrophic activity in winter in coastal NW Mediterranean Sea waters, *Journal of plankton research*, 36(1),
243-258, doi:10.1093/plankt/ftb073, 2014.

793
794 Le Hir P., Cayocca F., and Waeles B.: Dynamics of sand and mud mixtures: A multiprocess-based modelling
strategy, *Continental Shelf Research*, 31(10), S135– S149, doi:10.1016/j.csr.2010.12.009, 2011.

795
796 Lehmuskero, A., Skogen Chauton, M., and Boström, T.: Light and photosynthetic microalgae: A review of
797 cellular- and molecular-scale optical processes, *Progress in Oceanography*, 168(September), 43–56,
doi:10.1016/j.pocean.2018.09.002, 2018.

798
799 Le Pape, O., and Menesguen, A.: Hydrodynamic prevention of eutrophication in the Bay of Brest (France), a
800 modelling approach, *Journal of Marine Systems*, 12(1-4), 171-186, doi:10.1016/S0924-7963(96)00096-6, 1997.

801
802 Liu, X., Dunne, J. P., Stock, C. A., Harrison, M. J., Adcroft, A., and Resplandy, L.: Simulating water residence
803 time in the coastal ocean: A global perspective, *Geophysical Research Letters*, 46(23), 13910-13919, doi:
804 10.1029/2019GL085097, 2019.

805 Ménesguen, A., Dussauze, M., and Dumas, F.: Designing optimal scenarios of nutrient loading reduction in a
806 WFD/MSFD perspective by using passive tracers in a biogeochemical-3D model of the English Channel/Bay of
807 Biscay area, *Ocean & Coastal Management*, 163, 37-53, doi:10.1016/j.ocecoaman.2018.06.005, 2018.
808

809 Ménesguen, A., Dussauze, M., Dumas, F., Thouvenin, B., Garnier, V., Lecornu, F., and Répécaud, M.: Ecological
810 model of the Bay of Biscay and English Channel shelf for environmental status assessment part 1: Nutrients,
811 phytoplankton and oxygen, *Ocean Modelling*, 133, 56-78, doi.org/10.1016/j.ocemod.2018.11.002, 2019.

812 Mengual B., Le Hir P., Cayocca F., and Garlan T.: Modelling fine sediment dynamics: Towards a common erosion
813 law for fine sand, mud and mixtures, *Water*, 9, 564, doi:10.3390/w9080564, 2017.

814 Mikaelyan, A., Chasovnikov, V., Kubryakov, A., and Stanichny, S.: Phenology and drivers of the winter-spring
815 phytoplankton bloom in the open Black Sea: The application of Sverdrup's hypothesis and its refinements,
816 *Progress in Oceanography*, 151, 163-176, doi:10.1016/j.pocean.2016.12.006, 2017.

817 Moncheva, S., Gotsis-Skretas, O., Pagoub, K., and Krasteva, A.: Phytoplankton Blooms in Black Sea and
818 Mediterranean Coastal Ecosystems Subjected to Anthropogenic Eutrophication: Similarities and
819 Differences, *Estuarine, Coastal and Shelf Science*, 53, 281-295, doi:10.1006/ecss.2001.0767, 2001.
820

821 Oliver, E., Donat, M., Burrows, M., Moore, P., Smale, D., Alexandra, L., Benthuisen, J., Feng, M., Sen Gupta, A.,
822 Hobday, A., Holbrook, N., Perkins-Kirkpatrick, S., Scannell, H., Straub, S. and Wernberg, T.: Longer and more
823 frequent marine heatwaves over the past century, *Nature communications*, 9 :1324, doi:10.1038/s41467-018-
824 03732-9, 2018.
825

826 Paerl, H. W., Hall, N. S., Peierls, B. L., and Rossignol, K. L.: Evolving paradigms and challenges in estuarine and
827 coastal eutrophication dynamics in a culturally and climatically stressed world, *Estuaries and coasts*, 37(2), 243-
828 258, doi.org/10.1007/s12237-014-9773-x, 2014.
829

830 Peierls, B. L., Hall, N. S., and Paerl, H. W.: Non-monotonic responses of phytoplankton biomass accumulation to
831 hydrologic variability: a comparison of two coastal plain North Carolina estuaries, *Estuaries and coasts*, 35(6),
832 1376-1392, doi.org/10.1007/s12237-012-9547-2, 2012.
833

834 Petton, S., Pouvreau, S., and Dumas, F. Intensive use of Lagrangian trajectories to quantify coastal area dispersion,
835 *Ocean Dynamics*, 70(4), 541-559, doi.org/10.1007/s10236-019-01343-6, 2020.
836

837 Philippart, C. J. M., van Iperen, J. M., Cadée, G. C., and Zuur, A. F.: Long-term field observations on seasonality
838 in chlorophyll-a concentrations in a shallow coastal marine ecosystem, the Wadden Sea, *Estuaries and Coasts*,
839 33(2), 286–294, doi:10.1007/s12237-009-9236-y, 2010.
840

841 Pingree, R.D. and Le Cann, B. Celtic and Armorican slope and shelf residual currents. *Progress in Oceanography*
842 23 (4), 303–338, doi:10.1016/0079-6611(89)90003-7, 1989.
843

844 Plus, M., Thouvenin, B., Andrieux, F., Dufois, F., Ratmaya, W., Souchu, P. Diagnostic étendu de l'eutrophisation
845 (DIETE). Modélisation biogéochimique de la zone Vilaine-Loire avec prise en compte des processus
846 sédimentaires. Description du modèle Bloom (Biogeochemical Coastal Ocean Model). RST/LER/MPL/21.15.
847 <https://archimer.ifremer.fr/doc/00754/86567/>, 2021.
848

849 Poppeschi, C., Charria, G., Goberville, E., Rimmelin-Maury, P., Barrier, N., Petton, S., Unterberger, M.,
850 Grossteffan, E., Repeccaud, M., Quémener, L., Le Roux, J.-F., and Tréguer, P.: Unraveling salinity extreme events
851 in coastal environments: a winter focus on the bay of Brest, *Frontiers in Marine Science*, 8,
852 705403, doi:10.3389/fmars.2021.705403, 2021.
853

854 Quéguiner, B., and Tréguer, P.: Studies on the Phytoplankton in the Bay of Brest (Western Europe), Seasonal
855 Variations in Composition, Biomass and Production in Relation to Hydrological and Chemical Features (1981—
856 1982), *Botanica Marina*, 27, 449-459, 1984.
857

858 Ragueneau, O., Quéguiner, B. and Tréguer, P.: Contrast in biological responses to tidally-induced vertical mixing
859 for two macrotidal ecosystems of western Europe, *Estuarine, Coastal and Shelf Science*, 42, 645-665,
860 doi:10.1006/ecss.1996.0042, 1996.
861

862 Ragueneau, O., Chauvaud, L., Leynaert, A., Thouzeau, G., Paulet, Y. M., Bonnet, S., Lorrain, A., Grall, J.,
863 Corvaisier, R., Le Hir, M., Jean, F., and Clavier, J.: Direct evidence of a biologically active coastal silicate pump:
864 ecological implications, *Limnology and Oceanography*, 47(6), 1849-1854, doi.org/10.4319/lo.2002.47.6.1849,
865 2002.

866
867 Ragueneau, O., Raimonet, M., Mazé, C., Coston-Guarini, J., Chauvaud, L., Danto, A., Grall, J., Jean, F., Paulet
868 Y.-M., and Thouzeau, G.: The impossible sustainability of the Bay of Brest ? Fifty years of ecosystem changes,
869 interdisciplinary knowledge construction and key questions at the science-policy-community interface, *Frontiers*
870 *in Marine Science*, 5, 124, doi.org/10.3389/fmars.2018.00124, 2018.

871
872 Ratmaya, W., Soudant, D., Dalmon-Monviola, J., Plus, M., Cochennec-Laureau, N., Goubert, E., Andrieux-Loyer,
873 F., Barillé, L. and Souchu, P.: Reduced phosphorus loads from the Loire and Vilaine rivers were accompanied by
874 increasing eutrophication in the Vilaine Bay (south Brittany, France), *Biogeosciences*, 16:1361-1380,
875 doi:10.5194/bg-16-1361-2019, 2019.

876
877 Ratmaya, W., Laverman, AM., Rabouille, C., Akbarzadeh, Z., Andrieux-Loyer, F., Barillé, L., Barillé, A-L., Le
878 Merrer, Y., and Souchu, P.: Temporal and spatial variations in benthic nitrogen cycling in a temperate macro-tidal
879 coastal ecosystem : Observation and modeling, *Continental Shelf Research*, doi:10.1016/j.csr.2022.104649, 2022.

880
881 Répécaud, M., Quemener, L., Charria, G., Pairaud, I., Rimmelin, P., Claquin, P., Jacqueline, F., Lefebvre, A.,
882 Facq, J.V., Retho, M., and Verney, R.: National observation infrastructure: an example of a fixed-platforms
883 network along the French Coast: COAST HF, OCEANS IEE, pp. 1-6, doi:10.1109/OCEANSE.2019.8867451,
884 2019.

885
886 REPHY: French Observation and Monitoring program for Phytoplankton and Hydrology in coastal waters,
887 REPHY dataset - French Observation and Monitoring program for Phytoplankton and Hydrology in coastal waters.
888 Metropolitan data, SEANOE, doi:10.17882/47248, 2021.

889
890 Retho, M., Quemener, L., Le Gall, C., Repecaud, M., Souchu, P., Gabellec, R. and Manach, S.: MOLIT Vilaine
891 data and metadata from Coriolis Data Centre, SEANOE, doi:10.17882/46529, 2020.

892
893 Rimmelin-Maury, P., Charria, G., Repecaud, M., Quemener, L., Beaumont, L. Guillot, A., Gautier, L., Prigent, S.,
894 Le Becque, T., Bihannic, I., Bonnat, A., Le Roux, J-F., Grossteffan, E., Devesa, J., and Bozec, Y.: Iroise buoys
895 data from Coriolis data center as core parameter support for Brest Bay and Iroise sea studies, SEANOE, 2020.

896
897 Rossignol-Strick, M.: A marine anoxic event on the Brittany coast, July 1982, *Journal of Coastal Research*, 11-
898 20, <https://www.jstor.org/stable/4297005>, 1985.

899
900 Rumyantseva, A., Henson, S., Martin, A., Thompson, A. F., Damerell, G. M., Kaiser, J., and Heywood, K. J.:
901 Phytoplankton spring bloom initiation: The impact of atmospheric forcing and light in the temperate North
902 Atlantic, *Ocean. Progress in oceanography*, 178, 102202, doi:10.1016/j.pocean.2019.102202, 2019.

903
904 Saeck, E. A., Hadwen, W. L., Rissik, D., O'Brien, K. R., and Burford, M. A.: Flow events drive patterns of
905 phytoplankton distribution along a river–estuary–bay continuum, *Marine and Freshwater Research*, 64(7), 655-
906 670, doi:10.1071/MF12227, 2013.

907
908 Sathyendranath, S., Ji, R., and Browman, H. I.: Revisiting Sverdrup's critical depth hypothesis, *ICES Journal of*
909 *Marine Science*, 72(6), 1892-1896, doi:10.1093/icesjms/fsv110, 2015.

910
911 Schlegel, R. W., Darmaraki, S., Benthuyssen, J. A., Filbee-Dexter, K., and Oliver, E. C.: Marine cold-
912 spells, *Progress in Oceanography*, 198, 102684, doi.org/10.1101/2021.10.18.464880, 2021.

913
914 Serre-Fredj, L., Jacqueline, F., Navon, M., Izabel, G., Chasselín, L., Jolly, O., ... and Claquin, P.: Coupling high
915 frequency monitoring and bioassay experiments to investigate a harmful algal bloom in the Bay of Seine (French-
916 English Channel), *Marine Pollution Bulletin*, 168, 112387, doi:10.1016/j.marpolbul.2021.112387, 2021.

917
918 Smetacek, V., & Cloern, J. E.: On phytoplankton trends, *Science*, 319(5868), 1346-1348, doi:
919 10.1126/science.1151330, 2008.

920
921 Sommer, U., Adrian, R., De Senerpont Domis, L., Elser, J. J., Gaedke, U., Ibelings, B., Jeppesen, E., Lürling, M.,
922 Molinero, J. C., Mooij, W. M., van Donk, E., and Winder, M.: Beyond the Plankton Ecology Group (PEG) model:
923 mechanisms driving plankton succession, *Annual review of ecology, evolution, and systematics*, 43, 429-448,
924 doi:10.1146/annurev-ecolsys-110411-160251, 2012.
925
926 Stockwell, J. D., Doubek, J. P., Adrian, R., Anneville, O., Carey, C. C., Carvalho, L., ... and Wilson, H. L.: Storm
927 impacts on phytoplankton community dynamics in lakes, *Global change biology*, 26(5), 2756-2784,
928 doi:10.1111/gcb.15033, 2020.
929
930 Sverdrup, H.: On vernal blooming of phytoplankton, *Conseil Exp. Mer*, 18, 287-295, 1953.
931
932 Thyssen, M., Tarran, G. A., Zubkov, M. V., Holland, R. J., Grégori, G., Burkill, P. H., and Denis, M.: The
933 emergence of automated high-frequency flow cytometry: revealing temporal and spatial phytoplankton variability,
934 *Journal of plankton research*, 30(3), 333-343, doi:10.1093/plankt/fbn005, 2008.
935
936 Tian, T., Merico, A., Su, J., Staneva, J., Wiltshire, K., and Wirtz, K.: Importance of resuspended sediment
937 dynamics for the phytoplankton spring bloom in a coastal marine ecosystem, *Journal of Sea Research*, 62(4), 214-
938 228, doi:10.1016/j.seares.2009.04.001, 2009.
939
940 Tian, T., Su, J., Flöser, G., Wiltshire, K., and Wirtz, K.: Factors controlling the onset of spring blooms in the
941 German Bight 2002–2005: light, wind and stratification, *Continental Shelf Research*, 31(10), 1140-1148,
942 doi:10.1016/j.csr.2011.04.008, 2011.
943
944 Townsend, D. W., Cammen, L. M., Holligan, P. M., Campbell, D. E., and Pettigrew, N. R.: Causes and
945 consequences of variability in the timing of spring phytoplankton blooms, *Deep Sea Research Part I:
946 Oceanographic Research Papers*, 41(5-6), 747-765, doi:10.1016/0967-0637(94)90075-2, 1994.
947
948 Trombetta, T., Vidussi, F., Mas, S., Parin, D., Simier, M., and Mostajir, B.: Water temperature drives
949 phytoplankton blooms in coastal waters, *PloS one*, 14(4), e0214933, doi:10.1371/journal.pone.0214933, 2019.
950
951 Wiltshire, K. H., Malzahn, A. M., Wirtz, K., Greve, W., Janisch, S., Mangelsdorf, P., ... and Boersma, M.:
952 Resilience of North Sea phytoplankton spring bloom dynamics: An analysis of long-term data at Helgoland
953 Roads, *Limnology and Oceanography*, 53(4), 1294-1302, doi:10.4319/lo.2008.53.4.1294, 2008.
954
955 Wiltshire, K. H., Boersma, M., Carstens, K., Kraberg, A. C., Peters, S., and Scharfe, M.: Control of phytoplankton
956 in a shelf sea: determination of the main drivers based on the Helgoland Roads Time Series, *Journal of Sea
957 Research*, 105, 42-52, doi:10.1016/j.seares.2015.06.022, 2015.
958
959
960
961
962
963
964
965
966
967
968
969
970
971
972
973
974
975
976
977
978
979
980
981

982
 983
 984
 985
 986
 987
 988
 989
 990
 991
 992
 993
 994
 995
 996
 997
 998
 999
 1000
 1001
 1002
 1003
 1004
 1005
 1006
 1007
 1008
 1009
 1010
 1011
 1012
 1013
 1014
 1015
 1016
 1017
 1018
 1019
 1020
 1021
 1022
 1023
 1024
 1025
 1026
 1027
 1028
 1029

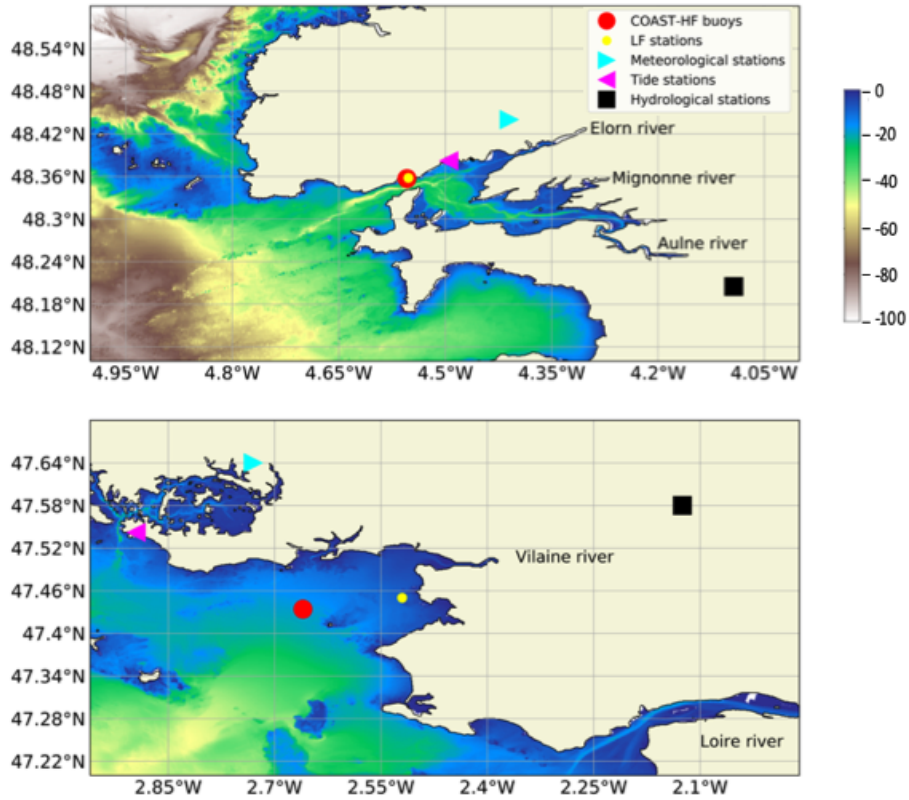


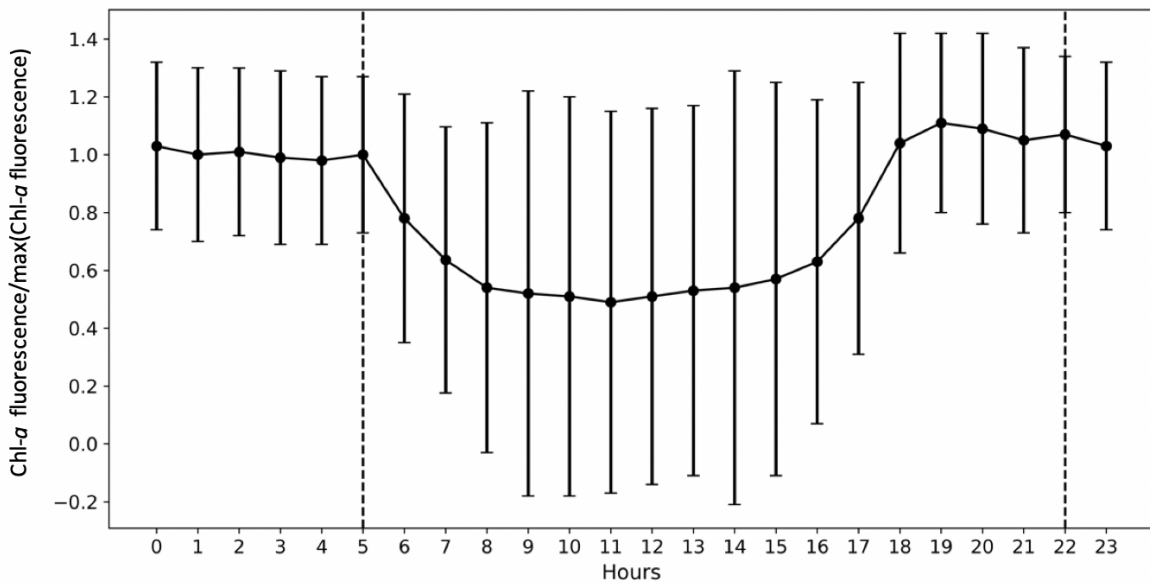
Figure 1: Location of the sampling sites: COAST-HF-Iroise and COAST-HF-Molit buoys (red circles); SOMLIT-Brest and REPHY-Loscolo sampling stations (yellow circles); Brest and Crouesty tide gauge stations (blue triangles); Guipavas and Vannes-Séné meteorological stations (purple triangles); hydrological stations of the Aulne and Vilaine rivers (black squares) with the Loire station off the map.

Parameters	Bay of Brest	Bay of Vilaine
Dissolved O ₂ ($mg L^{-1}$)	9	10
Mesozooplankton ($\mu mol N L^{-1}$)	0.05	0.1
Microzooplankton ($\mu mol N L^{-1}$)	0.05	0.05
Dinoflagellates ($\mu mol N L^{-1}$)	0.05	0.1
Diatoms ($\mu mol N L^{-1}$)	0.5	0.5
Soluble reactive phosphorus ($\mu mol L^{-1}$)	0.5	0.8
Silicic acid ($\mu mol L^{-1}$)	10	30

Nitrate ($\mu\text{mol L}^{-1}$)	16	30
Ammonium ($\mu\text{mol L}^{-1}$)	0.5	0.25
Coarse sand (g L^{-1})	0	0
Fine sand (g L^{-1})	0	0
Mud (g L^{-1})	0.03	0.05

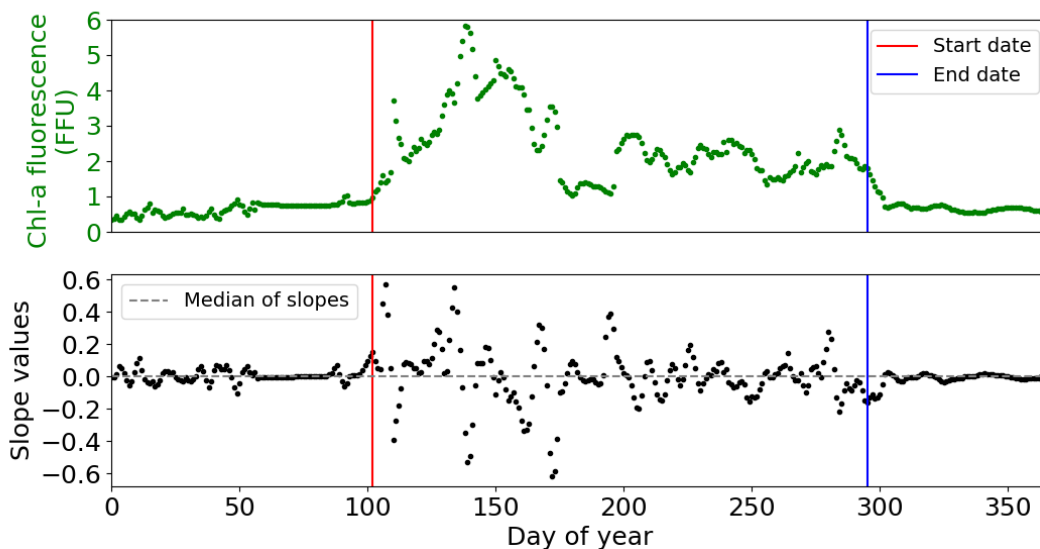
1030
1031
1032
1033

Table 1: Initial conditions in the water column for the MARS-1DV model for the beginning of the simulation on the February 15th.



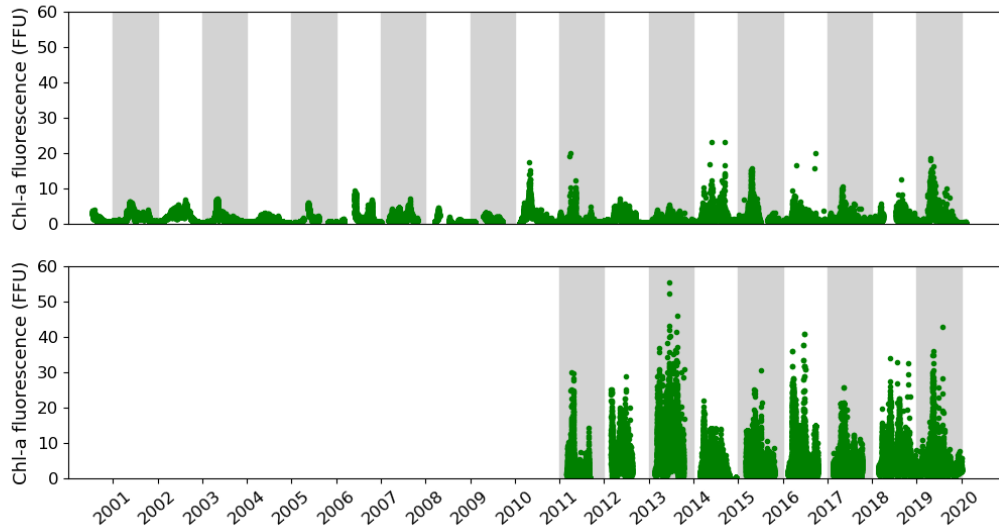
1034
1035
1036
1037
1038

Figure 2: Importance of the Quenching effect on Chl-*a* fluorescence is represented by COAST-HF-Iroise data from 2000 to 2019. The standard deviation is represented by vertical black bars. The dashed lines represent the beginning and end of the selected values for the rest of the study from 10 pm to 5 am.



1039
1040
1041
1042

Figure 3: Example of detection of the start (red line) and end (blue line) of the phytoplankton growing period in 2001 at COAST-HF-Iroise. The threshold value - median of slopes - is represented by a dotted grey line.



1043
1044
1045
1046
1047
1048

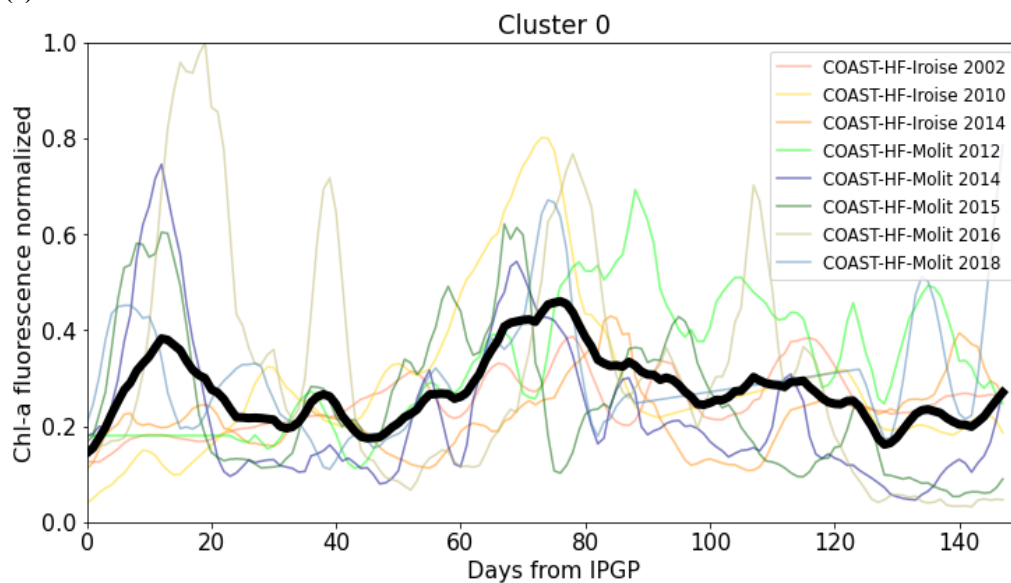
Figure 4: Temporal changes in the *in situ* Chl-*a* fluorescence measured in the Bay of Brest (top) and the Bay of Vilaine (bottom).

	Start date (Day of year)	End date (Day of year)	Duration (Days)	Cumulative Chl- <i>a</i> fluorescence (FFU)
	<i>Min - Median - Max</i>	<i>Min - Median - Max</i>	<i>Min - Median - Max</i>	<i>Min - Median - Max</i>
Bay of Brest (2001-2019)	50 - 69 - 102	253 - 274 - 308	165 - 200 - 256	217 - 364 - 567
Bay of Vilaine (2011-2019)	53 - 68 - 93	218 - 269 - 316	165 - 179 - 239	276 - 582 - 1406

1049
1050
1051
1052
1053
1054
1055

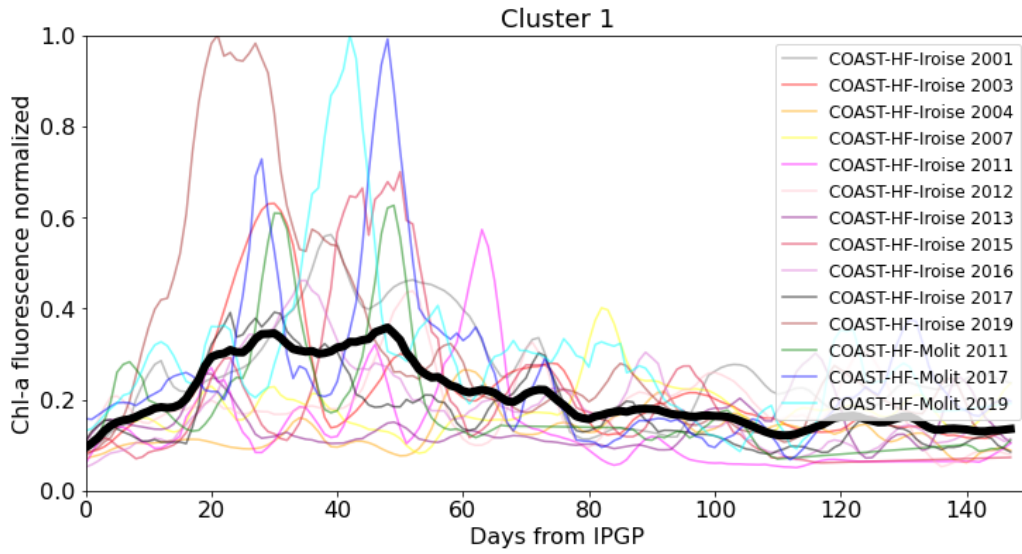
Table 2: Global characteristics of the phytoplankton growing period in the Bay of Brest and in the Bay of Vilaine.

(a)



1056
1057
1058

1059 (b)
1060



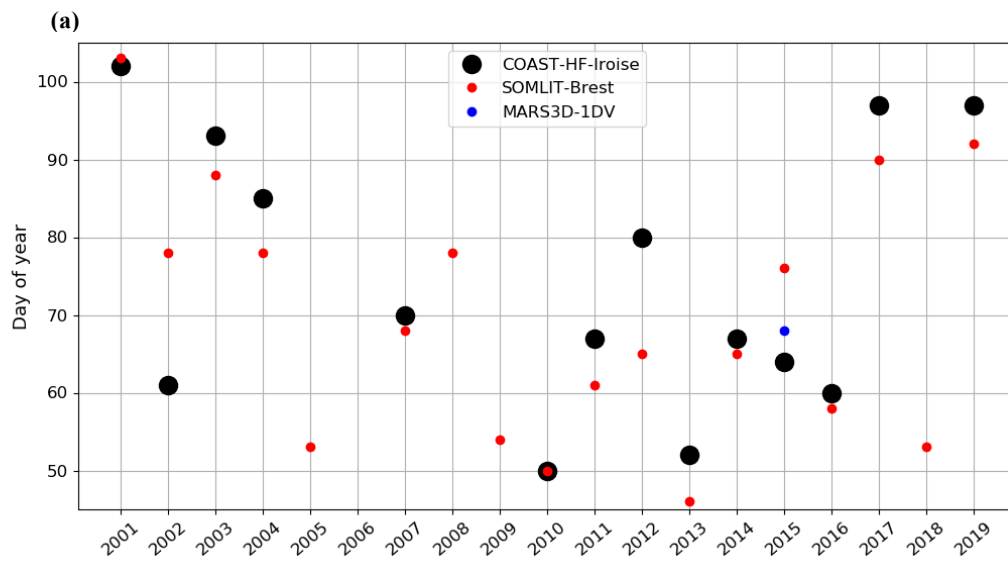
1061
1062
1063
1064
1065
1066
1067

Figure 5: (a) Cluster 0 and (b) cluster 1 representative of the patterns of the phytoplankton growing period observed in both bays. The median pattern is drawn in bold.

Year	2001	2002	2003	2004	2005	2006	2007	2008	2009	2010	2011	2012	2013	2014	2015	2016	2017	2018	2019
Bay of Brest COAST-HF-Iroise	1	0	1	1			1			0	1	1	1	0	1	1	1		1
Bay of Vilaine COAST-HF-Molit											1	0	X	0	0	0	1	0	1

1068
1069
1070
1071
1072
1073
1074

Table 3: Cluster group assigned to each annual phytoplankton growing period on both sites. Grey boxes represent years with missing data. The cross represents the year 2013 of the Bay of Vilaine not considered.



1075
1076
1077
1078

(b)

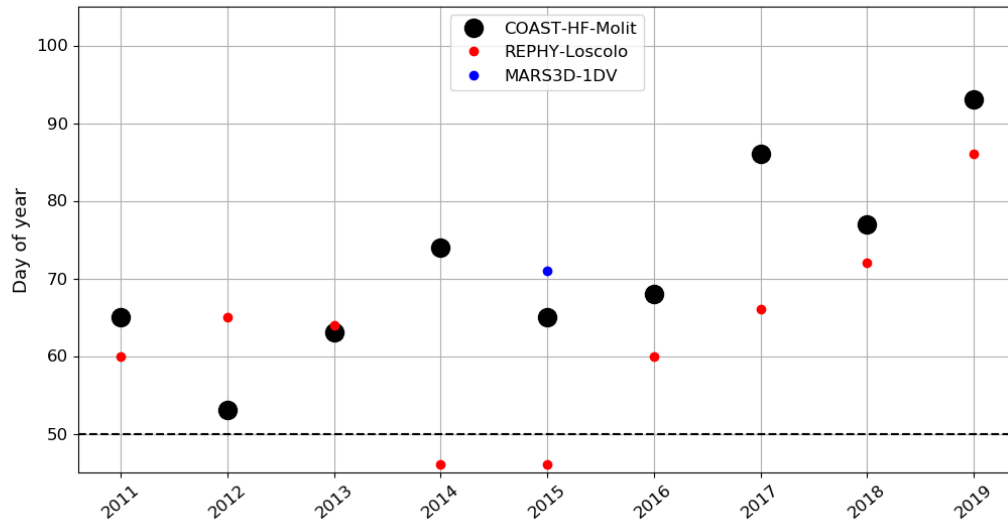
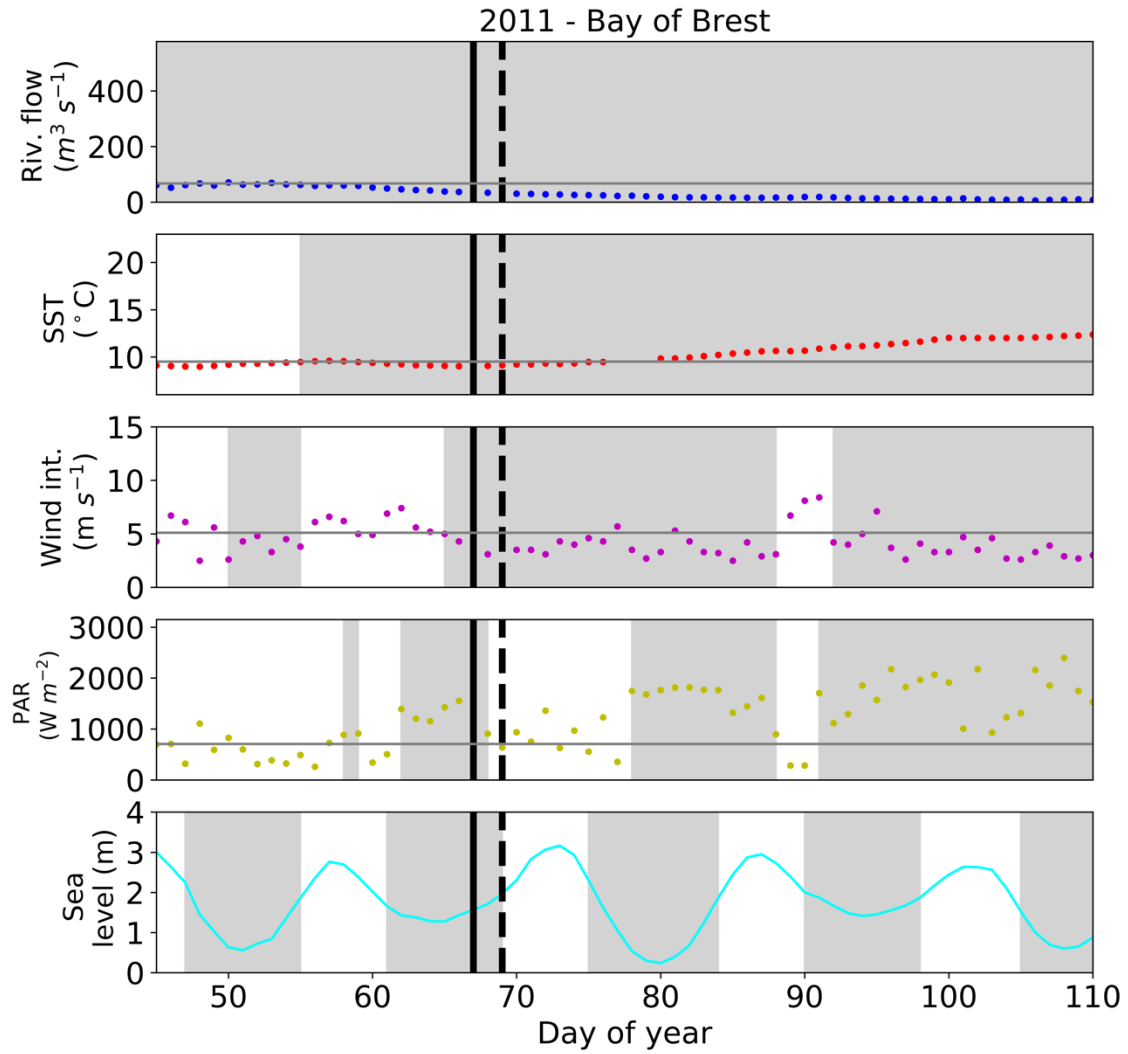


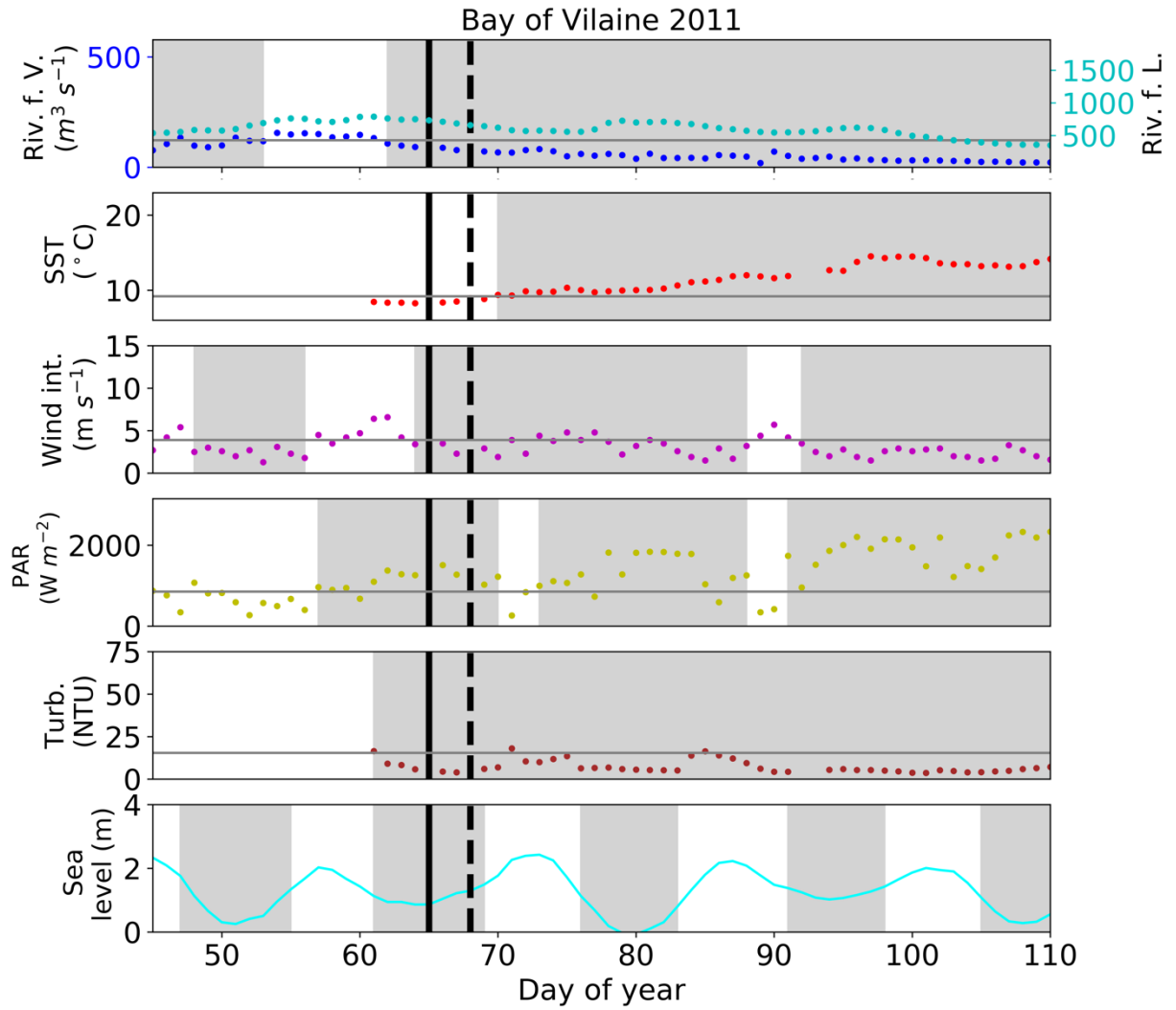
Figure 6: Changes in the IGP date in (a) the Bay of Brest and (b) the Bay of Vilaine are determined with high-frequency time series (black circles), low-frequency time series (red circles) and with the model (blue circle). The dotted black line represents the date of the COAST-HF-Molit buoy deployment.

1079
 1080
 1081
 1082
 1083
 1084
 1085
 1086
 1087
 1088
 1089
 1090
 1091
 1092
 1093
 1094
 1095
 1096
 1097
 1098
 1099
 1100
 1101
 1102
 1103
 1104
 1105
 1106
 1107
 1108
 1109
 1110
 1111
 1112
 1113
 1114
 1115
 1116
 1117
 1118
 1119
 1120
 1121
 1122
 1123
 1124
 1125
 1126
 1127



1129
 1130
 1131
 1132
 1133
 1134
 1135
 1136
 1137
 1138
 1139
 1140
 1141
 1142
 1143
 1144
 1145
 1146
 1147
 1148
 1149
 1150
 1151

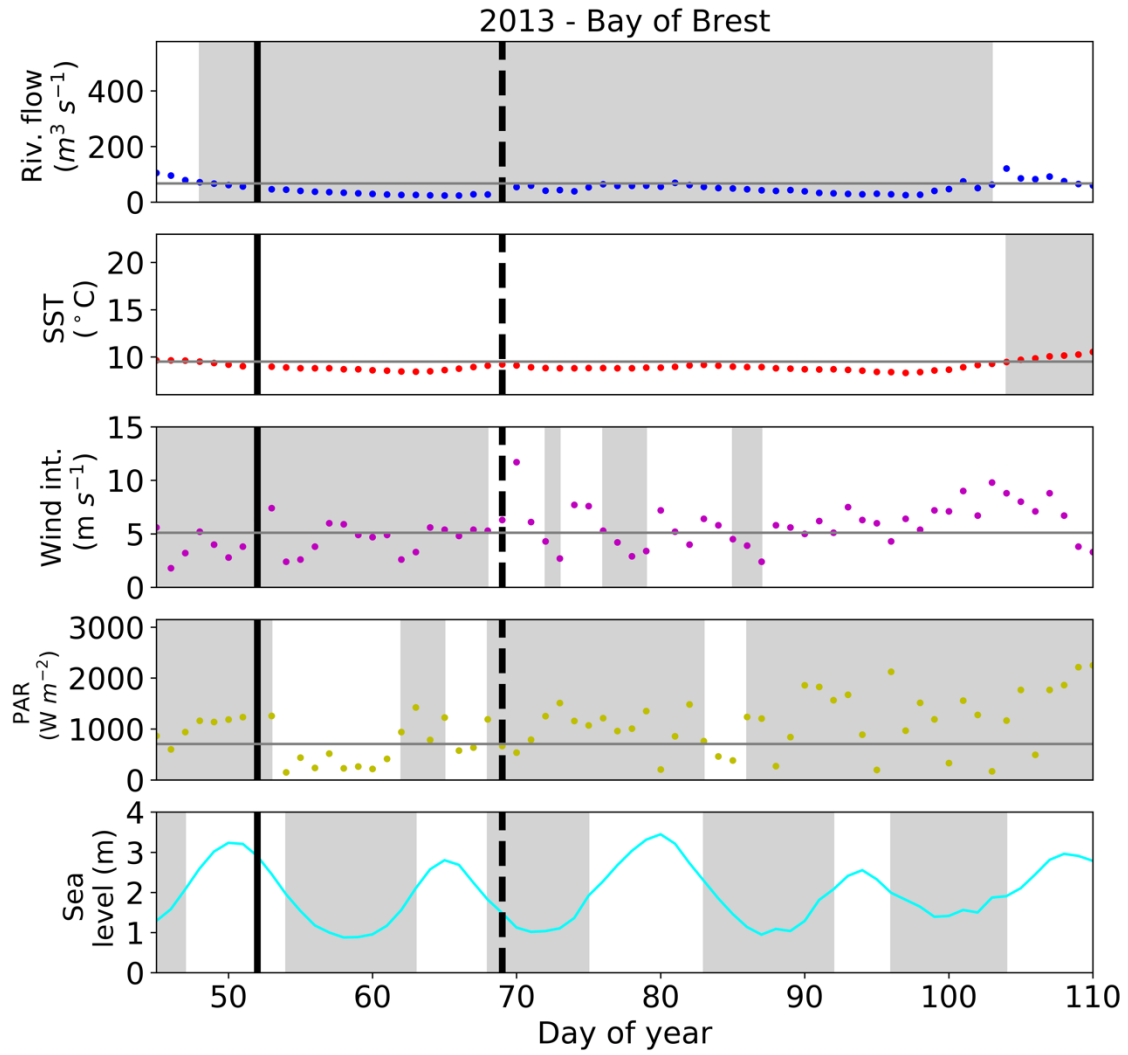
1152 (b)



1153
1154
1155
1156
1157
1158
1159
1160
1161
1162
1163
1164
1165
1166
1167
1168
1169
1170
1171
1172
1173
1174
1175

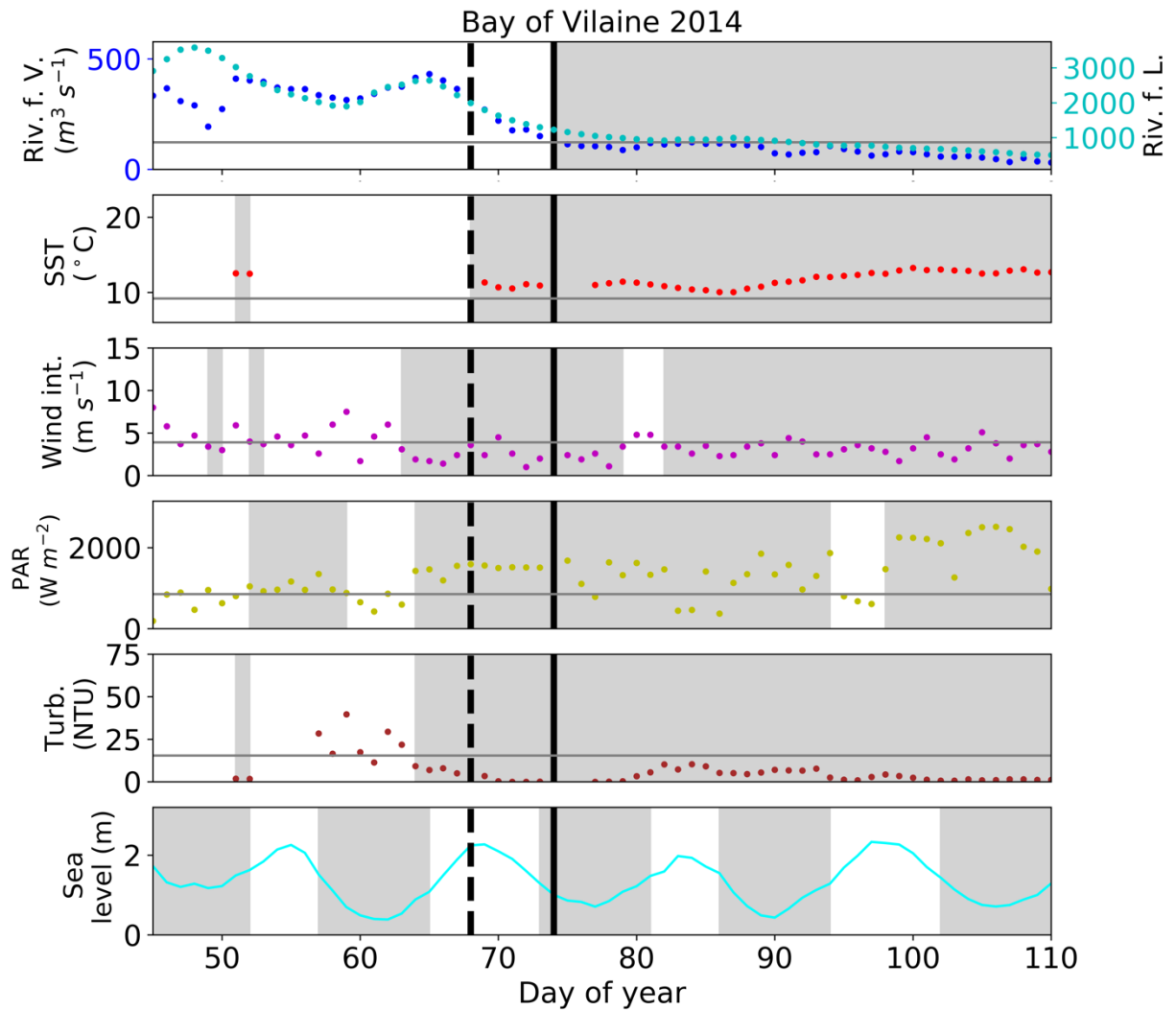
1176
1177
1178

(c)



1179
1180
1181
1182
1183
1184
1185
1186
1187
1188
1189
1190
1191
1192
1193
1194
1195
1196
1197
1198
1199

1200 (d)



1201
1202
1203
1204
1205
1206
1207
1208
1209
1210
1211

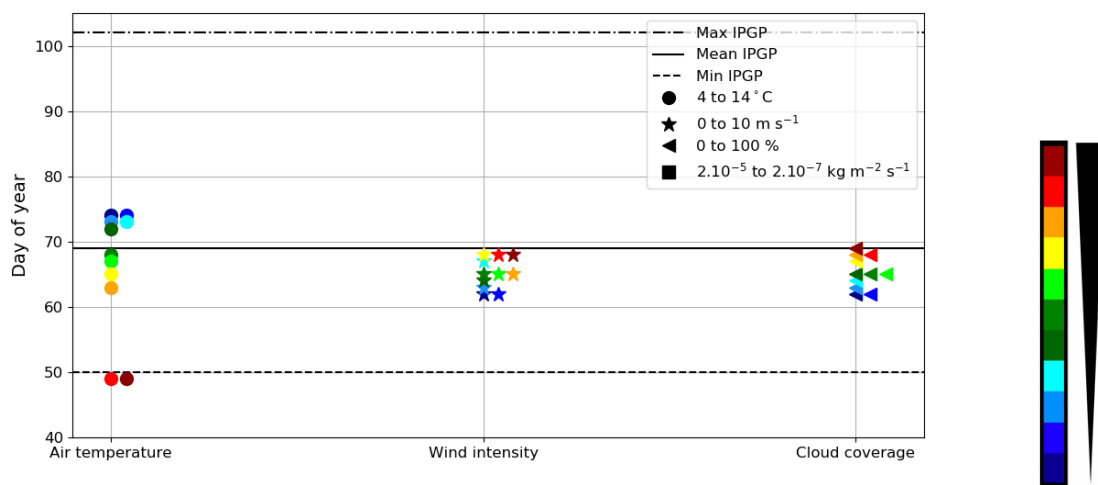
Figure 7: IPGP dates and environmental drivers: flow of the Aulne, Vilaine and Loire rivers, Sea Surface Temperature, wind intensity, PAR, turbidity and sea level at high tide. Illustrations in 2011 for a mean IPGP date in (a) the Bay of Brest and (b) the Bay of Vilaine; in 2013 for an early IPGP date in (c) the Bay of Brest; in 2014 for a late IPGP date in (d) the Bay of Vilaine. The mean IPGP date of each bay is represented by a dotted black line and the IPGP date of the year is represented by a straight black line. Thresholds of each environmental driver are represented by grey vertical lines corresponding to the mean conditions calculated 30 days around the IPGP date. Grey areas are time periods favorable to IPGP.

	Bay of Brest (2001-2019)	Bay of Vilaine (2011-2019)
	<i>Min - Median - Max</i>	<i>Min - Median - Max</i>
River flow (m ³ s ⁻¹)	13 - 46 - 100	36 - 96 - 205
SST (°C)	8 - 10 - 12	8 - 10 - 11
Wind intensity (m s ⁻¹)	1 - 3 - 6	1 - 3 - 4
PAR (W m ⁻²)	915 - 1373 - 2220	814 - 1341 - 1939
Turbidity (NTU)	1 - 7 - 21	0 - 7 - 22
Sea level (m)	0.5 - 1.6 - 2.9	0.6 - 0.9 - 1.6
PO₄ (μmol/L)	0.1 - 0.4 - 0.6	0.1 - 0.8 - 1.4
DIN (μmol/L)	8 - 20 - 38	25 - 57 - 244
Si(OH)₄ (μmol/L)	4 - 8 - 16	8 - 38 - 112

Table 4: Characteristics of environmental drivers at the date of IPGP except for nutrients from January to March in the Bay of Brest and in the Bay of Vilaine.

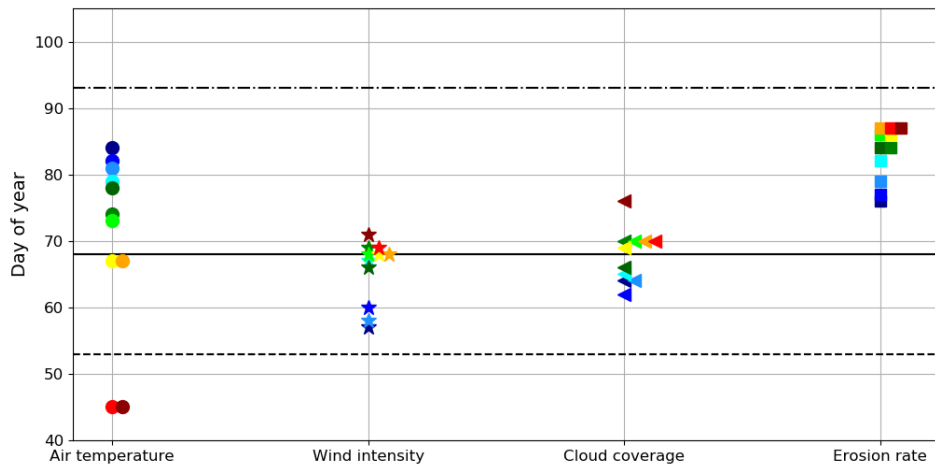
1212
1213
1214
1215
1216
1217
1218
1219

(a)



1220
1221
1222

(b)



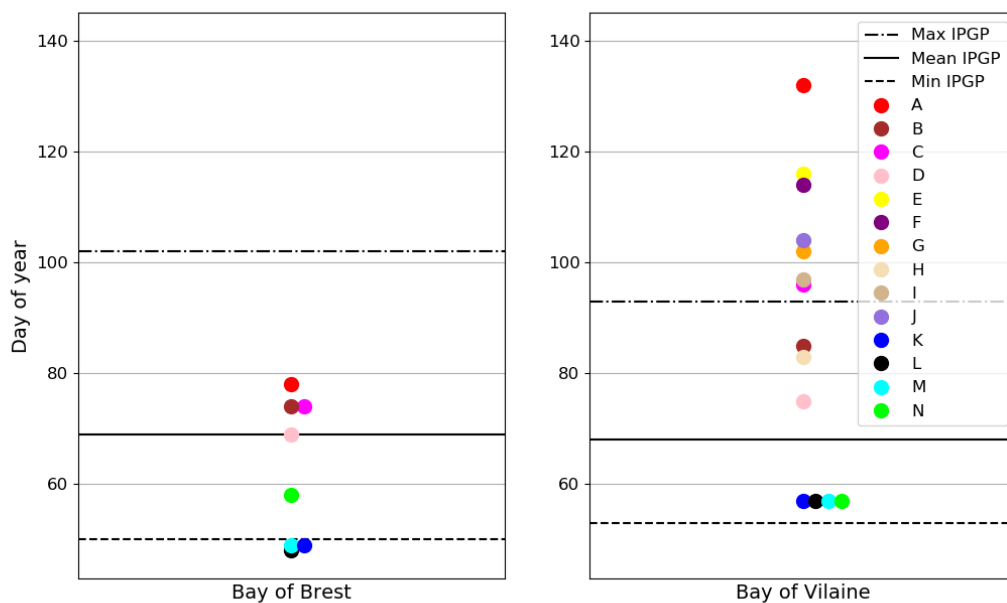
1223
1224
1225
1226
1227
1228
1229
1230

Figure 8: Impact of the variation of environmental drivers on the date of IPGP in (a) the Bay of Brest and (b) the Bay of Vilaine. Steps of: 1°C for the air temperature, 1 m s⁻¹ for the wind intensity, 10 % for the cloud coverage and 0.0000036 kg m⁻² s⁻¹ for the erosion rate equivalent to a variation of suspended matter between 0.02 and 0.08 mg L⁻¹ at IPGP.

Experiment	Air temperature (°C)	Wind intensity (m s ⁻¹)	Cloud coverage (%)	Erosion rate (kg m ⁻² s ⁻¹)	Simulated IPGP Bay of Brest (days)	Simulated IPGP Bay of Vilaine (days)
1	4	3	70	2.10 ⁻⁶	+5	+16
2	14	3	70	2.10 ⁻⁶	-20	-23
3	10	0	70	2.10 ⁻⁶	-1	-11
4	10	10	70	2.10 ⁻⁶	-7	+3
5	10	3	0	2.10 ⁻⁶	=	-4
6	10	3	100	2.10 ⁻⁶	-7	+8
7	10	3	70	2.10 ⁻⁷		+8
8	10	3	70	2.10 ⁻⁵		+19
A	4	10	100	2.10 ⁻⁵	+9	+64
B	4	10	70	2.10 ⁻⁶	+5	+17
C	4	3	100	2.10 ⁻⁶	+5	+28
D	10	10	100	2.10 ⁻⁶	=	+6
E	4	10	70	2.10 ⁻⁵		+48
F	4	3	100	2.10 ⁻⁵		+46
G	10	10	100	2.10 ⁻⁵		+34
H	10	3	100	2.10 ⁻⁵		+19
I	10	10	70	2.10 ⁻⁵		+29
J	4	3	70	2.10 ⁻⁵		+36
K	14	0	0	2.10 ⁻⁷	-20	-11
L	14	0	70	2.10 ⁻⁷	-21	-11
M	14	3	0	2.10 ⁻⁷	-20	-11
N	10	0	0	2.10 ⁻⁷	-11	-11

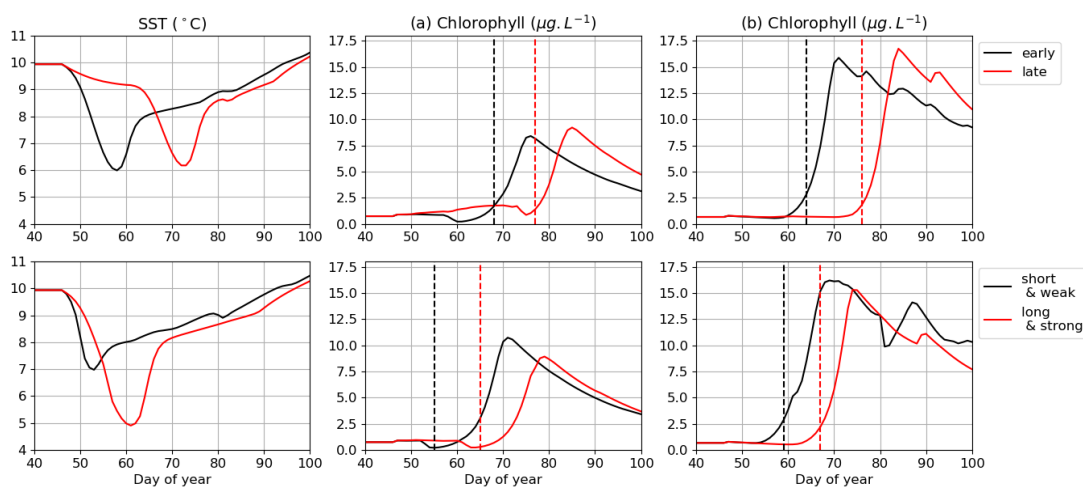
1231
1232
1233
1234

Table 5: Assumptions are explored in the 1DV model for environmental parameters independently (1-8) and with combined effect (A-N) with the modified values (grey background) and text in bold for the Bay of Brest only (+ for later IPGP, - for earlier IPGP, = for equal IPGP) with IPGP equal the mean observed IPGP of day 68.



1235
1236
1237
1238

Figure 9: Influence of combined environmental parameters for the MARS-1DV model in both bays (Bay of Brest - left and Bay of Vilaine - right) with detailed experiments in Table 2.



1239

1240
1241
1242
1243
1244
1245
1246
1247
1248
1249

Figure 10: Impact of cold spells on the IPGP date simulated in (a) the Bay of Brest and (b) the Bay of Vilaine. Four conditions of cold spells are explored: an early (mid-February), a late (end of February), a short (8 days) and a long (20 days). The IPGP dates are represented by dotted lines.